The Jellium

Riccardo Fantoni*

Università di Trieste,
Dipartimento di Fisica,
strada Costiera 11,
34151 Grignano (Trieste),
Italy

(Dated: December 12, 2017)

We present the main computer experiment results for Jellium. Either in its ground state and at finite temperatures.

CONTENTS

* rfantoni@ts.infn.it

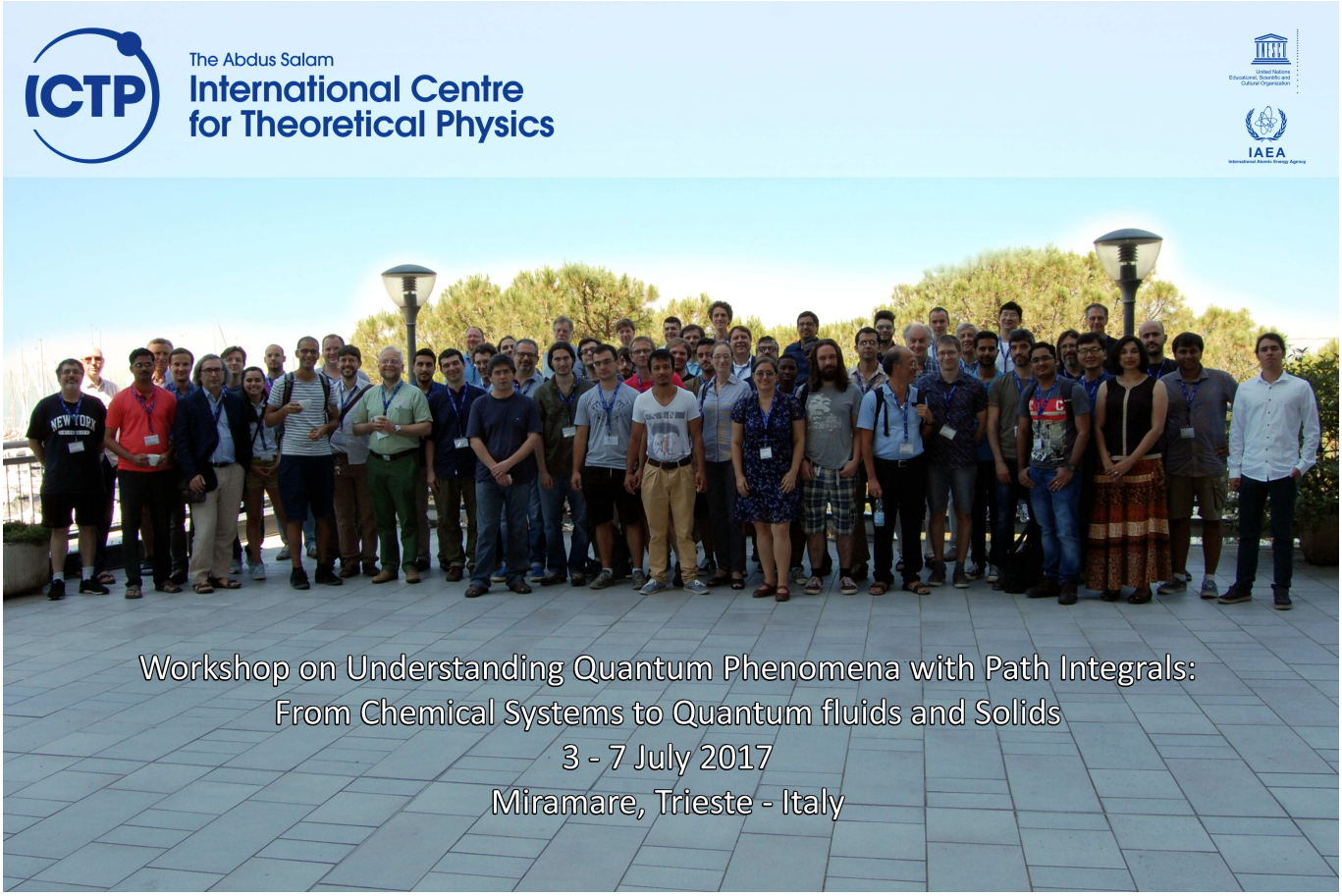

I. THE MODEL

The *Jellium* model of Wigner (Ichimaru, 1982; March and Tosi, 1984; Martin, 1988; Singwi and Tosi, 1981) is an assembly of N_+ spin up pointwise electrons and N_- spin down pointwise electrons of charge e moving in a positive inert background that ensures charge neutrality. The total number of electrons is $N = N_+ + N_-$ and the average particle number density is $n = N/\Omega$, where Ω is the volume of the electron fluid. In the volume Ω there is a uniform

neutralizing background with a charge density $\rho_b = -en$. So that the total charge of the system is zero. The fluid polarization is then $\xi = |N_+ - N_-|/N$: $\xi = 0$ in the unpolarized (paramagnetic) case and $\xi = 1$ in the fully polarized (ferromagnetic) case.

Setting lengths in units of $a = (4\pi n/3)^{-1/3}$ and energies in Rydberg's units, $\mathrm{Ry} = \hbar^2/2ma_0^2$, where m is the electron mass and $a_0 = \hbar^2/me^2$ is the Bohr radius, the Hamiltonian of Jellium is

$$\mathcal{H} = -\frac{1}{r_s^2}\sum_{i=1}^{N}\boldsymbol{\nabla}_{\mathbf{r}_i}^2 + V(R) \ , \tag{1.1}$$

$$V = \frac{1}{r_s}\left(2\sum_{i<j}\frac{1}{|\mathbf{r}_i - \mathbf{r}_j|} + \sum_{i=1}^{N} r_i^2 + v_0\right) \ , \tag{1.2}$$

where $R = (\mathbf{r}_1, \mathbf{r}_2, \ldots, \mathbf{r}_N)$ with $\mathbf{r}_i$ the coordinate of the ith electron, $r_s = a/a_0$, and v_0 a constant containing the self energy of the background.

The kinetic energy scales as $1/r_s^2$ and the potential energy (particle-particle, particle-background, and background-background interaction) scales as $1/r_s$, so for small r_s (high electronic densities), the kinetic energy dominates and the electrons behave like an ideal gas. In the limit of large r_s, the potential energy dominates and the electrons crystallize into a Wigner crystal (Wigner, 1934). No liquid phase is realizable within this model since the pair-potential has no attractive parts even though a superconducting state (Leggett, 1975) may still be possible (see chapter 8.9 of Ref. (Giuliani and Vignale, 2005) and Ref. (Pollock and Ceperley, 1987)).

The Jellium has been solved either by integral equation theories in its ground state (Singwi *et al.*, 1968) or by computer experiments in its ground state (Ceperley and Alder, 1980) and at finite temperature (Brown *et al.*, 2013).

Some details on the linear response theory for the Jellium can be found in appendixes 4 and 5 of Ref. (March and Tosi, 1984). Some details on the sum rules for the dielectric function can be found in appendix 6 of Ref. (March and Tosi, 1984). Some details on the moments of density fluctuation spectrum in the plasma can be found in appendix 7 of Ref. (March and Tosi, 1984). And some details on the Lindhard theory of dynamic screening can be found in appendix 8 of Ref. (March and Tosi, 1984).

A. Lindhard theory of static screening in Jellium ground state

Suppose we switch on an appropriately screened test charge potential δV, actually the so called Hartree potential, in a free electron gas. The Hartree potential $\delta V(\mathbf{r})$ created at a distance r from a static point charge of magnitude e at the origin, should be evaluated self-consistently from the Poisson equation,

$$\nabla^2\delta V(\mathbf{r}) = -4\pi e^2[\delta(\mathbf{r}) + \delta n(\mathbf{r})] \ , \tag{1.3}$$

where $\delta n(\mathbf{r})$ is the change in electronic density induced by the foreign charge. The electron density $n(\mathbf{r})$ may be written as

$$n(\mathbf{r}) = 2\sum_{\mathbf{k}} |\psi_{\mathbf{k}}(\mathbf{r})|^2 \ , \tag{1.4}$$

where $\psi_{\mathbf{k}}(\mathbf{r})$ are single-electron orbitals, the sum over $\mathbf{k}$ is restricted to occupied orbitals ($|\mathbf{k}| \leq k_F$, where k_F is the Fermi wave vector) and the factor 2 comes from the sum over spin orientations. We must now calculate how the orbitals in the presence of the foreign charge, differ from plane waves $\exp(i\mathbf{k}\cdot\mathbf{r})$. We use for this purpose the Schrödinger equation,

$$\nabla^2\psi_{\mathbf{k}}(\mathbf{r}) + [k^2 - \frac{2m}{\hbar^2}\delta V(r)]\psi_{\mathbf{k}}(\mathbf{r}) = 0 \ , \tag{1.5}$$

having imposed that the orbitals reduce to plane waves with energy $\hbar^2k^2/(2m)$ at large distance [1].

With the aforementioned boundary condition the Schrödinger equation may be converted into an integral equation,

$$\psi_{\mathbf{k}}(\mathbf{r}) = \frac{1}{\sqrt{\Omega}}e^{i\mathbf{k}\cdot\mathbf{r}} + \frac{2m}{\hbar^2}\int G_{\mathbf{k}}(\mathbf{r} - \mathbf{r}')\delta V(\mathbf{r}')\psi_{\mathbf{k}}(\mathbf{r}')d\mathbf{r}' \ , \tag{1.6}$$

[1] This approach (which lead to the Random Phase Approximation, RPA) is approximate insofar as the potential entering the Schrödinger equation has been taken as the Hartree potential, thus neglecting exchange and correlation between an incoming electron and the electronic screening cloud.

with $G_{\mathbf{k}}(\mathbf{r}) = -\exp(i\mathbf{k}\cdot\mathbf{r})/(4\pi r)$ and Ω the volume of the system.

Within linear response theory we can replace $\psi_{\mathbf{k}}(\mathbf{r})$ by $\Omega^{-1/2}\exp(i\mathbf{k}\cdot\mathbf{r})$ inside the integral. This yields

$$\delta n(\mathbf{r}) = -\frac{mk_F^2}{2\pi^3\hbar^2}\int j_1(2k_F|\mathbf{r}-\mathbf{r}'|)\frac{\delta V(\mathbf{r}')}{|\mathbf{r}-\mathbf{r}'|^2}d\mathbf{r}' \quad , \tag{1.7}$$

with $j_1(x)$ being the first-order spherical Bessel function $[\sin(x) - x\cos(x)]/x^2$. Using this result in the Poisson equation we get

$$\nabla^2\delta V(r) = -4\pi e^2\delta(\mathbf{r}) + \frac{2mk_F^2e^2}{\pi^2\hbar^2}\int j_1(2k_F|\mathbf{r}-\mathbf{r}'|)\frac{\delta V(\mathbf{r}')}{|\mathbf{r}-\mathbf{r}'|^2}d\mathbf{r}' \quad , \tag{1.8}$$

which is easily soluble in Fourier transform. Writing $\delta V(k) = 4\pi e^2/[k^2\varepsilon(k)]$ we find,

$$\varepsilon(k) = 1 + \frac{2mk_Fe^2}{\pi k^2\hbar^2}\left[1 + \frac{k_F}{k}\left(\frac{k^2}{4k_F^2} - 1\right)\ln\left|\frac{k-2k_F}{k+2k_F}\right|\right] \quad , \tag{1.9}$$

which is the static dielectric function in RPA.

For $k \to 0$ this expression gives $\varepsilon(k) \to 1 + k_{TF}^2/k^2$ with $k_{TF} = 3\omega_p^2/v_F^2$ (ω_p being the plasma frequency and v_F the Fermi velocity) i.e. the result of the Thomas-Fermi theory. However $\varepsilon(k)$ has a singularity at $k = \pm 2k_F$, where its derivative diverges logarithmically [2]. This singularity in $\delta V(k)$ determines, after Fourier transform, the behavior of $\delta V(r)$ at large r. $\delta V(r)$ turns out to be an oscillating function [3] rather than a monotonically decreasing function as in the Thomas-Fermi theory. Indeed,

$$\delta V(r) = \int\frac{d\mathbf{k}}{(2\pi)^3}\frac{4\pi e^2}{k^2\varepsilon(k)}e^{i\mathbf{k}\cdot\mathbf{r}} = \frac{e^2}{i\pi r}\int_{-\infty}^{\infty}dk\frac{e^{ikr}}{k\varepsilon(k)} \quad , \tag{1.10}$$

and the integrand has non-analytic behavior at $q = \pm 2k_F$,

$$\left[\frac{1}{k\varepsilon(k)}\right]_{k\to\pm 2k_F} = -A(k-(\pm)2k_f)\ln|k-(\pm)2k_F| + \text{regular terms} \quad , \tag{1.11}$$

with $A = (k_{TF}^2/4k_F^2)/(k_{TF}^2 + 8k_F^2)$. Hence,

$$\begin{aligned}\delta V(r)|_{r\to\infty} = -\frac{Ae^2}{i\pi r}\int_{-\infty}^{\infty}dk\, e^{ikr}[(k-2k_F)\ln|k-2k_F| \\ +(k+2k_F)\ln|k+2k_F|] = -2Ae^2\frac{\cos(2k_Fr)}{r^3} \quad .\end{aligned} \tag{1.12}$$

This result is based on a theorem on Fourier transforms [4], stating that the asymptotic behavior of $\delta V(r)$ is determined by the low-k behavior as well as the singularities of $\delta V(k)$. Obviously, in the present case the asymptotic contribution from the singularities is dominant over the exponential decay of Thomas-Fermi type. The result implies that the screened ion-ion interaction in a metal has oscillatory character and ranges over several shells of neighbors.

B. Ewald sums

Periodic boundary conditions are necessary for extrapolating results of the finite system to the thermodynamic limit. Suppose the bare pair-potential, in infinite space, is $v(r)$,

$$v(r) = \int\frac{d\mathbf{k}}{(2\pi)^3}\,e^{-i\mathbf{k}\cdot\mathbf{r}}\tilde{v}(k) \ , \quad \tilde{v}(k) = \int d\mathbf{r}\,e^{i\mathbf{k}\cdot\mathbf{r}}v(r) \ . \tag{1.13}$$

The *best* pair-potential of the finite system is given by

$$v_I(r) = \sum_{\mathbf{L}} v(|\mathbf{r}+\mathbf{L}|) - \tilde{v}(0)/\Omega \ . \tag{1.14}$$

---

[2] The discontinuity in the momentum distribution across the Fermi surface introduces a singularity in elastic scattering processes with momentum transfer equal to $2k_F$.

[3] J. Friedel, *N. Cimento Suppl.* **7**, 287 (1958).

[4] M. Lighthill, "Introduction to Fourier Analysis and Generalized Functions" (University Press, Cambridge 1958)

where the $\mathbf{L}$ sum is over the Bravais lattice of the simulation cell $\mathbf{L} = (m_x L, m_y L, m_z L)$ where m_x, m_y, m_z range over all positive and negative integers and $\Omega = L^3$. We have also added a uniform background of the same density but opposite charge. Converting this to k-space and using the Poisson sum formula we get

$$v_I(r) = \frac{1}{\Omega} \sum_{\mathbf{k}}{}' \tilde{v}(k) e^{-i\mathbf{k}\cdot\mathbf{r}} \ , \tag{1.15}$$

where the prime indicates that we omit the $\mathbf{k} = 0$ term; it cancels out with the background. The $\mathbf{k}$ sum is over reciprocal lattice vectors of the simulation box $\mathbf{k_n} = (2\pi n_x/L,\ 2\pi n_y/L,\ 2\pi n_z/L)$ where n_x, n_y, n_z range over all positive and negative integers.

Because both sums, Eq. (1.14) and Eq. (1.15), are so poorly convergent (Allen and Tildesley, 1987) we follow the scheme put forward by Natoli *et al.* (Natoli and Ceperley, 1995) for approximating the image potential by a sum in k-space and a sum in r-space,

$$v_a(\mathbf{r}) = \sum_{\mathbf{L}} v_s(|\mathbf{r} + \mathbf{L}|) + \sum_{|\mathbf{k}| \le k_c} v_l(k) e^{i\mathbf{k}\cdot\mathbf{r}} - \tilde{v}(0)/\Omega \ , \tag{1.16}$$

where $v_s(r)$ is chosen to vanish smoothly as r approaches r_c, where r_c is less than half of the distance across the simulation box in any direction. If either r_c or k_c go to infinity then $v_a \to v_I$. Natoli *et al.* show that in order to minimize the error in the potential, it is appropriate to minimize $\chi^2 = \int_\Omega [v_I(r) - v_a(r)]^2 \, d\mathbf{r}/\Omega$. And choose for $v_s(r)$ an expansion in a fixed number of radial functions. This same technique has also been applied to treat the pseudo-potential described in section II.C.1.

Now let us work with N particles of charge e in a periodic box and let us compute the total potential energy of the unit cell. Particles i and j are assumed to interact with a potential $e^2 v(r_{ij}) = e^2 v(|\mathbf{r}_i - \mathbf{r}_j|)$. The potential energy for the N particle system is

$$V = \sum_{i<j} e^2 v_I(r_{ij}) + \sum_i e^2 v_M \ , \tag{1.17}$$

where $v_M = \frac{1}{2} \lim_{r\to 0} [v_I(r) - v(r)]$ is the interaction of a particle with its own images; it is a Madelung constant (March and Tosi, 1984) for particle i interacting with the perfect lattice of the simulation cell. If this term were not present, particle i would only see $N - 1$ particles in the surrounding cells instead of N.

II. JELLIUM IN ITS GROUND STATE

The ground state properties of Jellium has been for the first time found by Ceperley and Alder (Ceperley and Alder, 1980) through a diffusion Monte Carlo method (Kolorenc and Mitas, 2011). Since then better wave-functions and optimization methods have been developed, better schemes to minimize finite-size effect have been devised, and vastly improved computational facilities are available. Today, new modern techniques are available to optimize Slater-Jastrow wave-functions (Foulkes *et al.*, 2001) with backflow and three-body correlations (Kwon *et al.*, 1998) and Helmann and Feynman (HF) measures (Toulouse *et al.*, 2007) to calculate the RDF, particularly the on-top value, which suffers from poor statistical sampling in its conventional histogram implementation. Other useful tools are the twist-averaged boundary conditions (Lin *et al.*, 2001) and RPA-based corrections (Chiesa *et al.*, 2006) to minimize finite-size effects.

A. Monte Carlo simulation (Diffusion)

Consider the Schrödinger equation for the many-body wave-function, $\phi(R, t)$ (the wave-function can be assumed to be real, since both the real and imaginary parts of the wave-function separately satisfy the Schrödinger equation), in imaginary time, with a constant shift E_T in the zero of the energy. This is a diffusion equation in a $3N$-dimensional space (Anderson, 1976). If E_T is adjusted to be the ground-state energy, E_0, the asymptotic solution is a steady state solution, corresponding to the ground-state eigenfunction $\phi_0(R)$ (provided $\phi(R, 0)$ is not orthogonal to ϕ_0).

Solving this equation by a random-walk process with branching is inefficient, because the branching rate, which is proportional to the total potential $V(R)$, can diverge to $+\infty$. This leads to large fluctuations in the weights of the diffusers and to slow convergence when calculating averages. However, the fluctuations, and hence the statistical uncertainties, can be greatly reduced (Kalos *et al.*, 1974) by the technique of importance sampling (Hammersley and Handscomb, 1964).

One simply multiplies the Schrödinger equation by a known trial wave-function $\Psi(R)$ that approximate the unknown ground-state wave-function, and rewrites it in terms of a new probability distribution

$$f(R,t) = \phi(R,t)\Psi(R) \ , \tag{2.1}$$

whose normalization is given in Eq. (B1). This leads to the following diffusion equation

$$-\frac{\partial f(R,t)}{\partial t} = -\lambda \boldsymbol{\nabla}^2 f(R,t) + [E_L(R) - E_T] f(R,t) + \lambda \boldsymbol{\nabla} \cdot [f(R,t)\mathbf{F}(R)] \ . \tag{2.2}$$

Here $\lambda = \hbar^2/(2m)$, t is the imaginary time measured in units of $\hbar$, $E_L(R) = [H\Psi(R)]/\Psi(R)$ is the local energy of the trial wave-function, and

$$\mathbf{F}(R) = \boldsymbol{\nabla} \ln \Psi^2(R) \ . \tag{2.3}$$

The three terms on the right hand side of Eq. (2.2) correspond, from left to right, to diffusion, branching, and drifting, respectively.

At sufficiently long times the solution to Eq. (2.2) is

$$f(R,t) \approx N_0 \Psi(R) \phi_0(R) \exp[-(E_0 - E_T)t] \ , \tag{2.4}$$

where $N_0 = \int \phi_0(R)\phi(R,0)\, dR$. If E_T is adjusted to be E_0, the asymptotic solution is a stationary solution and the average $\langle E_L(R) \rangle_f$ of the local energy over the stationary distribution gives the ground-state energy E_0. If we set the branching to zero $E_L(R) = E_T$ then this average would be equal to the expectation value $\int \Psi(R) H \Psi(R)\, dR$, since the stationary solution to Eq. (2.2) would then be $f = f_{\rm vmc} = \Psi^2$. In other words, without branching we would obtain the variational energy of Ψ, rather than E_0, as in a Variational Monte Carlo (VMC) calculation.

The time evolution of $f(R,t)$ is given by

$$f(R^{'}, t+\tau) = \int dR G(R^{'}, R; \tau) f(R,t) \ , \tag{2.5}$$

where the Green's function $G(R^{'}, R; \tau) = \Psi(R')\langle R'| \exp[-\tau(H - E_T)]|R\rangle \Psi^{-1}(R)$ is a transition probability for moving the set of coordinates from R to $R^{'}$ in a time τ. Thus G is a solution of the same differential equation, Eq. (2.2), but with the initial condition $G(R^{'}, R; 0) = \delta(R^{'} - R)$. For short times τ an approximate solution for G is

$$G(R^{'}, R; \tau) = (4\pi\lambda\tau)^{-3N/2} e^{-|R' - R - \lambda\tau \mathbf{F}(R)|^2/4\lambda\tau} e^{-\tau\{[E_L(R) + E_L(R')]/2 - E_T\}} + O(\tau^2) \ . \tag{2.6}$$

To compute the ground-state energy and other expectation values, the N-particle distribution function $f(R,t)$ is represented, in diffusion Monte Carlo, by an average over a time series of generations of walkers each of which consists of a fixed number of n_w walkers. A walker is a pair $(R_\alpha, \omega_\alpha)$, $\alpha = 1, 2, \ldots, n_w$, with R_α a $3N$-dimensional particle configuration with statistical weight ω_α. At time t, the walkers represent a random realization of the N-particle distribution, $f(R,t) = \sum_{\alpha=1}^{n_w} \omega_\alpha^t \delta(R - R_\alpha^t)$. The ensemble is initialized with a VMC sample from $f(R,0) = \Psi^2(R)$, with $\omega_\alpha^0 = 1/n_w$ for all α. Note that if the trial wave-function were the exact ground-state then there would be no branching and it would be sufficient $n_w = 1$. A given walker (R^t, ω^t) is advanced in time (diffusion and drift) as $R^{t+\tau} = R^t + \chi + \lambda\tau \boldsymbol{\nabla} \ln \Psi^2(R^t)$ where χ is a normally distributed random $3N$-dimensional vector with variance $2\lambda\tau$ and zero mean (Kalos and Whitlock, 2008). In order to satisfy detailed balance we accept the move with a probability $A(R, R'; \tau) = \min[1, W(R, R')]$, where $W(R, R') = [G(R, R'; \tau)\Psi^2(R')]/[G(R', R; \tau)\Psi^2(R)]$. This step would be unnecessary if G were the exact Green's function, since W would be unity. Finally, the weight ω_α^t is replaced by $\omega_\alpha^{t+\tau} = \omega_\alpha^t \Delta\omega_\alpha^t$ (branching), with $\Delta\omega_\alpha^t = \exp\{-\tau[(E_L(R_\alpha^t) + E_L(R_\alpha^{t+\tau}))/2 - E_T]\}$.

However, for the diffusion interpretation to be valid, f must always be positive, since it is a probability distribution. But we know that the many-fermions wave-function $\phi(R,t)$, being antisymmetric under exchange of a pair of particles of the parallel spins, must have nodes, *i.e.* points R where it vanishes. In the fixed-nodes approximation one restricts the diffusion process to walkers that do not change the sign of the trial wave-function. One can easily demonstrate that the resulting energy, $\langle E_L(R) \rangle_f$, will be an upper bound to the exact ground-state energy; the best possible upper bound with the given boundary condition (Ceperley, 1991).

A detailed description of the algorithm used for the DMC calculation can be found in Ref. (Umrigar *et al.*, 1993).

B. Expectation values in DMC

In a DMC calculation there are various different possibilities to measure the expectation value of a physical observable, as for example the RDF. If $\langle\mathcal{O}\rangle_f$ is the measure and $\langle\ldots\rangle_f$ the statistical average over the probability distribution f we will, in the following, use the word *estimator* to indicate the function $\mathcal{O}$ itself, unlike the more common use of the word to indicate the usual Monte Carlo estimator $\sum_{i=1}^{\mathcal{N}}\mathcal{O}_i/\mathcal{N}$ of the average, where $\{\mathcal{O}_i\}$ is the set obtained evaluating $\mathcal{O}$ over a finite number $\mathcal{N}$ of points distributed according to f. Whereas the average from different estimators must give the same result, the variance, the square of the statistical error, can be different for different estimators.

1. The local estimator and the extrapolated measure

To obtain ground-state expectation values of quantities $\mathcal{O}$ that do not commute with the Hamiltonian we introduce the local estimator $\mathcal{O}_L(R) = [\mathcal{O}\Psi(R)]/\Psi(R)$ and then compute the average over the DMC walk, the so called mixed measure, $\overline{\mathcal{O}}^{\rm mix} = \langle\mathcal{O}_L(R)\rangle_f = \int\phi_0(R)\mathcal{O}\Psi(R)\,dR/\int\phi_0(R)\Psi(R)\,dR$. This is inevitably biased by the choice of the trial wave-function. A way to remedy to this bias is the use of the forward walking method (Barnett *et al.*, 1991; Liu *et al.*, 1974) or the reptation quantum Monte Carlo method (Baroni and Moroni, 1999) to reach pure estimates. Otherwise this bias can be made of leading order δ^2, with $\delta = \phi_0 - \Psi$, introducing the extrapolated measure

$$\overline{\mathcal{O}}^{\rm ext} = 2\overline{\mathcal{O}}^{\rm mix} - \overline{\mathcal{O}}^{\rm var}\ , \tag{2.7}$$

where $\overline{\mathcal{O}}^{\rm var} = \langle\mathcal{O}_L\rangle_{f_{\rm vmc}}$ is the variational measure. If the mixed measure equals the variational measure then the trial wave-function has maximum overlap with the ground-state.

2. The Hellmann and Feynman measure

Toulouse *et al.* (Assaraf and Caffarel, 2003; Toulouse *et al.*, 2007) observed that the *zero-variance* property of the energy (Ceperley and Kalos, 1979) can be extended to an arbitrary observable, $\mathcal{O}$, by expressing it as an energy derivative through the use of the Hellmann-Feynman theorem.

In a DMC calculation the Hellmann-Feynman theorem takes a form different from the one in a VMC calculation. Namely we start with the eigenvalue expression $(H^\lambda - E^\lambda)\Psi^\lambda = 0$ for the ground-state of the perturbed Hamiltonian $H^\lambda = H + \lambda\mathcal{O}$, take the derivative with respect to λ, multiply on the right by the ground-state at $\lambda = 0$, ϕ_0, and integrate over the particle coordinates to get

$$\int dR\,\phi_0(H^\lambda - E^\lambda)\frac{\partial\Psi^\lambda}{\partial\lambda} = \int dR\,\phi_0\left(\frac{\partial E^\lambda}{\partial\lambda} - \frac{\partial H^\lambda}{\partial\lambda}\right)\Psi^\lambda\ . \tag{2.8}$$

Then we notice that due to the Hermiticity of the Hamiltonian, at $\lambda = 0$ the left hand side vanishes, so that we get (Fantoni, 2013)

$$\left.\frac{\int dR\,\phi_0\mathcal{O}\Psi^\lambda}{\int dR\,\phi_0\Psi^\lambda}\right|_{\lambda=0} = \left.\frac{\partial E^\lambda}{\partial\lambda}\right|_{\lambda=0}\ . \tag{2.9}$$

This relation holds only in the $\lambda\to 0$ limit unlike the more common form (Landau and Lifshitz, 1977) which holds for any λ. Also it resembles Eq. (3) of Ref. (Gaudoin and Pitarke, 2007).

Given $E^\lambda = \int dR\phi_0(R)H^\lambda\Psi^\lambda(R)/\int dR\phi_0(R)\Psi^\lambda(R)$ the "Helmann and Feynman" (HF) measure in a DMC calculation is

$$\overline{\mathcal{O}}^{HF} = \left.\frac{dE^\lambda}{d\lambda}\right|_{\lambda=0} \approx \langle\mathcal{O}_L(R)\rangle_f + \langle\Delta\mathcal{O}_L^\alpha(R)\rangle_f + \langle\Delta\mathcal{O}_L^\beta(R)\rangle_f\ . \tag{2.10}$$

The α correction is (Fantoni, 2013)

$$\Delta\mathcal{O}_L^\alpha(R) = \left[\frac{H\Psi'}{\Psi'} - E_L(R)\right]\frac{\Psi'(R)}{\Psi(R)}\ . \tag{2.11}$$

This expression coincides with Eq. (18) of Ref. (Toulouse *et al.*, 2007). In a VMC calculation this term, usually, does not contribute to the average, with respect to $f_{\rm vmc} = \Psi^2$, due to the Hermiticity of the Hamiltonian. This is of

course not true in a DMC calculation. We will then define a Hellmann and Feynman variational (HFv) estimator as $\mathcal{O}^{HFv} = \mathcal{O}_L(R) + \Delta\mathcal{O}_L^{\alpha}(R)$. The β correction is (Fantoni, 2013)

$$\Delta\mathcal{O}_L^{\beta}(R) = [E_L(R) - E_0]\frac{\Psi'(R)}{\Psi(R)} \ , \tag{2.12}$$

where $E_0 = E^{\lambda=0}$. Which differs from Eq. (19) of Ref. (Toulouse *et al.*, 2007) by a factor of one half. This term is necessary in a DMC calculation not to bias the measure. The extrapolated Hellmann and Feynman measure will then be

$$\overline{\mathcal{O}}^{\text{HF-ext}} = 2\overline{\mathcal{O}}^{\text{HF}} - \langle\mathcal{O}^{\text{HFv}}\rangle_{f_{\text{vmc}}} \ . \tag{2.13}$$

Both corrections α and β to the local estimator depends on the *auxiliary* function, $\Psi' = \partial\Psi^{\lambda}/\partial\lambda|_{\lambda=0}$. Of course if we had chosen $\Psi^{\lambda=0}$, on the left hand side of Eq. (2.10), as the exact ground state wave-function, ϕ_0, instead of the trial wave-function, then both corrections would have vanished. When the trial wave-function is sufficiently close to the exact ground state function a good approximation to the auxiliary function can be obtained from first order perturbation theory for $\lambda \ll 1$. So the Hellmann and Feynman measure is affected by the new source of bias due to the choice of the auxiliary function independent from the bias due to the choice of the trial wave-function.

It is convenient to rewrite Eqs. (2.11) and (2.12) in terms of the logarithmic derivative $Q(R) = \Psi'(R)/\Psi(R)$ as follows

$$\Delta\mathcal{O}_L^{\alpha}(R) = -\frac{1}{r_s^2}\sum_{k=1}^{N}[\boldsymbol{\nabla}_{\mathbf{r}_k}^2 Q(R) + 2\mathbf{v}_k(R)\cdot\boldsymbol{\nabla}_{\mathbf{r}_k} Q(R)] \ , \tag{2.14}$$

$$\Delta\mathcal{O}_L^{\beta}(R) = [E_L(R) - E]Q(R) \ , \tag{2.15}$$

where $\mathbf{v}_k(R) = \boldsymbol{\nabla}_{\mathbf{r}_k}\ln\Psi(R)$ is the drift velocity of the trial wave-function. For each observable a specific form of Q has to be chosen.

C. Trial wave-function

We chose the trial wave-function of the Bijl-Dingle-Jastrow (Bijl, 1940; Dingle, 1949; Jastrow, 1955) or product form

$$\Psi(R) \propto D(R)\exp\left(-\sum_{i<j}u(r_{ij})\right) \ . \tag{2.16}$$

The function $D(R)$ is the exact wave-function of the non-interacting fermions (the Slater determinant) and serves to give the trial wave-function the desired antisymmetry

$$D(R) = \frac{1}{\sqrt{N_+!}}\det(\varphi_{n,m}^{+})\frac{1}{\sqrt{N_-!}}\det(\varphi_{n,m}^{-}) \ , \tag{2.17}$$

where for the fluid phase $\varphi_{n,m}^{\sigma} = e^{i\mathbf{k}_n\cdot\mathbf{r}_m}\delta_{\sigma_m,\sigma}/\sqrt{\Omega}$ with $\mathbf{k}_n$ a reciprocal lattice vector of the simulation box such that $|\mathbf{k}_n| \le k_F^{\sigma}$, σ the z-component of the spin ($\pm 1/2$), $\mathbf{r}_m$ the coordinates of particle m, and σ_m its spin z-component. For the unpolarized fluid there are two separate determinants for the spin-up and the spin-down states because the Hamiltonian is spin independent. For the polarized fluid there is a single determinant. For the general case of N_+ spin-up particles the polarization will be $\xi = |N_+ - N_-|/N$ and the Fermi wave-vector for the spin-up (spin-down) particles will be $k_F^{\pm} = (1\pm\xi)^{1/3}k_F$ with $k_F = (3\pi^2 n)^{1/3} = (9\pi/4)^{1/3}/(a_0 r_s)$ the Fermi wave-vector of the paramagnetic fluid. On the computer we fill closed shells so that N_σ is always odd. We only store $\mathbf{k}_n$ for each pair $(\mathbf{k}_n, -\mathbf{k}_n)$ and use sines and cosines instead of $\exp(i\mathbf{k}_n\cdot\mathbf{r}_i)$ and $\exp(-i\mathbf{k}_n\cdot\mathbf{r}_j)$.

The second factor (the Jastrow factor) includes in an approximate way the effects of particle correlations, through the "pseudo-potential", $u(r)$, which is repulsive.

In the crystal phase, the orbitals are Gaussians centered around body-centered-cubic lattice sites with a width chosen variationally.

1. The pseudo-potential

Here we will consider a system where the particles interact with a bare potential

$$v_\mu(r) = \frac{\mathrm{erf}(\mu r)}{r}, \tag{2.18}$$

whose Fourier transform is

$$\tilde{v}_\mu(k) = \frac{4\pi}{k^2} e^{-k^2/4\mu^2}, \tag{2.19}$$

so that for $\mu \to \infty$ we recover the Jellium and in the opposite limit $\mu \to 0$ we recover the non-interacting electron gas.

Neglecting the cross term between the Jastrow and the Slater determinant in Eq. (B6) (third term) and the Madelung constant, the variational energy per particle can be approximated as follows,

$$e_V = \frac{\langle E_L(R)\rangle_f}{N} = \frac{\int \Psi(R) H \Psi(R)\, dR}{N} \approx e_F + \frac{1}{2\Omega} {\sum_{\mathbf{k}}}' [e^2 \tilde{v}_\mu(k) - 2\lambda k^2 \tilde{u}(k)][S(k) - 1] + \\ \frac{1}{N\Omega^2} {\sum_{\mathbf{k},\mathbf{k}'}}' \lambda \mathbf{k}\cdot\mathbf{k}' \tilde{u}(k)\tilde{u}(k') \langle \rho_{\mathbf{k}+\mathbf{k}'} \rho_{-\mathbf{k}} \rho_{-\mathbf{k}'} \rangle_f + \dots \ , \tag{2.20}$$

where $e_F = (3/5)\lambda \sum_\sigma N_\sigma (k_F^\sigma)^2/N$ is the non-interacting fermions energy per particle, $\tilde{u}(k)$ is the Fourier transform of the pseudo-potential $u(r)$, $\tilde{v}_\mu(k) = 4\pi \exp(-k^2/4\mu^2)/k^2$ is the Fourier transform of the bare pair-potential, $S(k)$ is the static structure factor for a given $u(r)$ (see Sec. II.D.3), $\rho_{\mathbf{k}} = \sum_{i=1}^N \exp(i\mathbf{k}\cdot\mathbf{r}_i)$ is the Fourier transform of the total number density $\rho(\mathbf{r}) = \sum_i \delta(\mathbf{r} - \mathbf{r}_i)$, and the trailing dots stand for the additional terms coming from the exclusion of the $j = k$ term in the last term of Eq. (B6). Next we make the Random Phase Approximation (Feynman, 1972) and we keep only the terms with $\mathbf{k} + \mathbf{k}' = \mathbf{0}$ in the last term. This gives

$$e_V \approx e_F + \frac{1}{2\Omega} {\sum_{\mathbf{k}}}' \Big\{ [e^2 \tilde{v}_\mu(k) - 2\lambda k^2 \tilde{u}(k)][S(k) - 1] - 2n\lambda [k\tilde{u}(k)]^2 S(k) \Big\} + \dots \ . \tag{2.21}$$

In the limit $k \to 0$ we have to cancel the Coulomb singularity and we get $\tilde{u}^2(k) = m e^2 \tilde{v}_\mu(k)/(\hbar^2 n k^2) \simeq [(4\pi e^2/k^2)/(\hbar\omega_p)]^2$ (where $\omega_p = \sqrt{4\pi n e^2/m}$ is the plasmon frequency) or in adimensional units

$$\tilde{u}(k) = \sqrt{\frac{r_s}{3}} \frac{4\pi}{k^2} \ , \quad \text{small } k \ . \tag{2.22}$$

This determines the correct behavior of $\tilde{u}(k)$ as $k \to 0$ or the long range behavior of $u(r)$

$$u(r) = \sqrt{\frac{r_s}{3}} \frac{1}{r} \ , \quad \text{large } r \ . \tag{2.23}$$

Now to construct the approximate pseudo-potential, we start from the expression

$$\epsilon = e_F + \frac{1}{2\Omega} {\sum_{\mathbf{k}}}' [e^2 \tilde{v}_\mu(k) - \mathcal{A}\lambda k^2 \tilde{u}(k)][S(k) - 1] \ , \tag{2.24}$$

and use the following perturbation approximation, for how $S(k)$ depends on $\tilde{u}(k)$ (Gaskell, 1961, 1962),

$$\frac{1}{S(k)} = \frac{1}{S^x(k)} + \mathcal{B} n \tilde{u}(k) \ , \tag{2.25}$$

where $\mathcal{A}$ and $\mathcal{B}$ are constant to be determined and $S^x(k)$ the structure factor for the non-interacting fermions (see Eq. (D5)), which is $S^x = \sum_\sigma S^x_{\sigma,\sigma}$ with

$$S^x_{\sigma,\sigma}(k) = \begin{cases} \dfrac{n_\sigma}{n} \dfrac{y_\sigma}{2}(3 - y_\sigma^2) & y_\sigma < 1 \\ \dfrac{n_\sigma}{n} & \text{else} \end{cases} \tag{2.26}$$

where $n_\sigma = N_\sigma/\Omega$ and $y_\sigma = k/(2k_F^\sigma)$.

Minimizing ϵ with respect to $u(k)$, we obtain (Ceperley, 2004)

$$\mathcal{B}n\tilde{u}(k) = -\frac{1}{S^x(k)} + \left[\frac{1}{S^x(k)} + \frac{\mathcal{B}ne^2\tilde{v}_\mu(k)}{\lambda\mathcal{A}k^2}\right]^{1/2} , \tag{2.27}$$

This form is optimal at both long and short distances but not necessarily in between. In particular, for any value of ξ, the small k behavior of $\tilde{u}(k)$ is $\sqrt{2r_s/3\mathcal{A}\mathcal{B}}(4\pi/k^2)$ which means that

$$u(r) = \sqrt{\frac{2r_s}{3\mathcal{A}\mathcal{B}}}\frac{1}{r} , \quad \text{large } r . \tag{2.28}$$

The large k behavior of $\tilde{u}(k)$ is $(r_s/\mathcal{A})\tilde{v}_\mu(k)/k^2$, for any value of ξ, which in r space translates into

$$\left.\frac{du(r)}{dr}\right|_{r=0} = \begin{cases} -\dfrac{r_s}{2\mathcal{A}} & \mu \to \infty \\ 0 & \mu \text{ finite} \end{cases} \tag{2.29}$$

In order to satisfy the cusp condition for particles of antiparallel spins (any reasonable pseudo-potential has to obey to the cusp conditions (see Ref. (Foulkes *et al.*, 2001) Section IVF) which prevent the local energy from diverging whenever any two electrons ($\mu = \infty$) come together) we need to choose $\mathcal{A} = 1$, then the correct behavior at large r (2.22) is obtained fixing $\mathcal{B} = 2$ [5]. We will call this Jastrow $\mathcal{J}_1$ in the following.

It turns out that, at small μ, but not for the Coulomb case, a better choice is given by (Ceperley, 1978)

$$2n\tilde{u}(k) = -\frac{1}{S^x(k)} + \left[\left(\frac{1}{S^x(k)}\right)^2 + \frac{2ne^2\tilde{v}_\mu(k)}{\lambda k^2}\right]^{1/2} , \tag{2.30}$$

which still has the correct long (2.28) and short (2.29) range behaviors. We will call this Jastrow $\mathcal{J}_2$ in the following. This is expected since, differently from $\mathcal{J}_1$, $\mathcal{J}_2$ satisfies the additional exact requirement $\lim_{\mu\to 0} u(r) = 0$, as immediately follows from the definition (2.30). Then at small μ (and any r_s), the trial wave-function is expected to be very close to the stationary solution of the diffusion problem.

2. The backflow and three-body correlations

As shown in Appendix B, the trial wave-function of Eq. (2.16) can be further improved by adding three-body (3B) and backflow (BF) correlations (Kwon *et al.*, 1993, 1998) as follows

$$\Psi(R) = \tilde{D}(R)\exp\left[-\sum_{i<j}\tilde{u}(r_{ij}) - \sum_{l=1}^{N}\mathbf{G}(l)\cdot\mathbf{G}(l)\right] . \tag{2.31}$$

Here

$$\tilde{D}(R) = \frac{1}{\sqrt{N_+!}}\det(\tilde{\varphi}^+_{n,m})\frac{1}{\sqrt{N_-!}}\det(\tilde{\varphi}^-_{n,m}) , \tag{2.32}$$

with $\tilde{\varphi}^\sigma_{n,m} = e^{i\mathbf{k}_n\cdot\mathbf{x}_m}\delta_{\sigma_m,\sigma}/\sqrt{\Omega}$ and $\mathbf{x}_m$ quasi-particle coordinates defined as

$$\mathbf{x}_i = \mathbf{r}_i + \sum_{j\neq i}^{N}\eta(r_{ij})(\mathbf{r}_i - \mathbf{r}_j) . \tag{2.33}$$

The displacement of the quasi-particle coordinates $\mathbf{x}_i$ from the real coordinate $\mathbf{r}_i$ incorporates effects of hydrodynamic backflow (Feynman and Cohen, 1956), and changes the nodes of the trial wave-function. The backflow correlation function $\eta(r)$, is parametrized as (Kwon *et al.*, 1998)

$$\eta(r) = \lambda_B\frac{1 + s_B r}{r_B + w_B r + r^4} , \tag{2.34}$$

---

[5] Note that the probability distribution in a variational calculation is (from Eq. (2.16)) $\Psi^2(R) \propto D^2(R)\exp[-2U(R)]$ with $U(R) = \sum_{i<j}u(r_{ij})$. Then if one formally writes $D^2(R) = \exp[-2W(R)]$, Ψ^2 becomes the probability distribution for a classical fluid with potential $W + U$ at an inverse temperature $\beta = 2$. Then one sees that with the choice $\mathcal{B} = 2$, Eq (2.25) coincides with the well known Random Phase Approximation in the theory of classical fluids (see Ref. (Hansen and McDonald, 1986) Section 6.5) where W is the potential of the reference fluid and U the perturbation.

which has the long-range behavior $\sim 1/r^3$.

Three-body correlations are included through the vector functions

$$\mathbf{G}(i) = \sum_{j\neq i}^{N} \xi(r_{ij})(\mathbf{r}_i - \mathbf{r}_j) \ . \tag{2.35}$$

We call $\xi(r)$ the three-body correlation function which is parametrized as (Panoff and Carlson, 1989)

$$\xi(r) = a \exp\left\{-[(r-b)c]^2\right\} \ . \tag{2.36}$$

To cancel the two-body term arising from $\mathbf{G}(l)\cdot\mathbf{G}(l)$, we use $\tilde{u}(r) = u(r) - 2\xi^2(r)r^2$

The backflow and three-body correlation functions are then chosen to decay to zero with a zero first derivative at the edge of the simulation box.

D. The radial distribution function

The radial distribution function (RDF) is proportional to the probability of finding another particle of the fluid inside a spherical shell of radius r and thickness dr centered on any one particle on which you sit. This observable gives us informations about the structure of the fluid. We will see here how it can be measured in a DMC calculation. In appendix D we give some details on the determination of the RDF for the ideal gas and in appendix E we give some details on exact relationships that must be satisfied by the RDF of the interacting fluid, the *sum rules*.

1. Definition of the radial distribution function

The spin-resolved RDF is defined as (Feenberg, 1967; Hill, 1956)

$$g_{\sigma,\sigma'}(\mathbf{r},\mathbf{r}^{'}) = \frac{\left\langle \sum_{i,j\neq i} \delta_{\sigma,\sigma_i}\delta_{\sigma',\sigma_j}\delta(\mathbf{r}-\mathbf{r}_i)\delta(\mathbf{r}^{'}-\mathbf{r}_j)\right\rangle}{n_\sigma(\mathbf{r})n_{\sigma'}(\mathbf{r}^{'})} \ , \tag{2.37}$$

$$n_\sigma(\mathbf{r}) = \left\langle \sum_{i=1}^{N} \delta_{\sigma,\sigma_i}\delta(\mathbf{r}-\mathbf{r}_i)\right\rangle \ , \tag{2.38}$$

where here, and in the following, $\langle\ldots\rangle$ will denote the expectation value respect to the ground-state. Two exact conditions follow immediately from the definition: i. the zero-moment sum rule

$$\sum_{\sigma,\sigma'}\int d\mathbf{r}d\mathbf{r}'\, n_\sigma(\mathbf{r})n_\sigma(\mathbf{r}')[g_{\sigma,\sigma'}(\mathbf{r},\mathbf{r}^{'})-1] = -N \ , \tag{2.39}$$

also known as the charge (monopole) sum rule in the sequence of multipolar sum rules in the framework of charged fluids (Martin, 1988), ii. $g_{\sigma,\sigma}(\mathbf{r},\mathbf{r}) = 0$ due to the Pauli exclusion principle.

For the homogeneous and isotropic fluid $n_\sigma(\mathbf{r}) = N_\sigma/\Omega$ where N_σ is the number of particles of spin σ and $g_{\sigma,\sigma'}$ depends only on the distance $r = |\mathbf{r}-\mathbf{r}^{'}|$, so that

$$g_{\sigma,\sigma'}(r) = \frac{1}{4\pi r^2}\frac{\Omega}{N_\sigma N_{\sigma'}}\left\langle \sum_{i,j\neq i}\delta_{\sigma,\sigma_i}\delta_{\sigma',\sigma_j}\delta(r-r_{ij})\right\rangle \ . \tag{2.40}$$

The total (spin-summed) radial distribution function will be

$$\begin{aligned} g(r) &= \frac{1}{n^2}\sum_{\sigma,\sigma'} n_\sigma n_{\sigma'} g_{\sigma,\sigma'}(r) \\ &= \left(\frac{1+\xi}{2}\right)^2 g_{+,+}(r) + \left(\frac{1-\xi}{2}\right)^2 g_{-,-}(r) + \frac{1-\xi^2}{2}g_{+,-}(r) \ . \end{aligned} \tag{2.41}$$

2. From the structure to the thermodynamics

As it is well known the knowledge of the RDF gives access to the thermodynamic properties of the system. The mean potential energy per particle can be directly obtained from $g(r)$ and the bare pair-potential $v_\mu(r)$ as follows

$$e_p = \sum_{\sigma,\sigma'} \frac{n_\sigma n_{\sigma'}}{2n} \int d\mathbf{r}\, e^2 v_\mu(r)[g_{\sigma,\sigma'}(r) - 1] \;, \tag{2.42}$$

where we have explicitly taken into account of the background contribution. Suppose that $e_p(r_s)$ is known as a function of the coupling strength r_s. The virial theorem for a system with Coulomb interactions ($v_\infty(r) = 1/r$) gives $N(2e_k + e_p) = 3P\Omega$ with $P = -d(Ne_0)/d\Omega$ the pressure and $e_0 = e_k + e_p$ the mean total ground-state energy per particle. We then find

$$e_p(r_s) = 2e_0(r_s) + r_s \frac{de_0(r_s)}{dr_s} = \frac{1}{r_s}\frac{d}{dr_s}[r_s^2 e_0(r_s)] \;, \tag{2.43}$$

which integrates to

$$e_0(r_s) = e_F + \frac{1}{r_s^2}\int_0^{r_s} dr'_s\, r'_s e_p(r'_s) \;. \tag{2.44}$$

We can rewrite the ground-state energy per particle of the ideal Fermi gas, in reduced units, as

$$e_F = \left(\frac{9\pi}{4}\right)^{2/3} \frac{3}{10}\phi_5(\xi)\frac{1}{r_s^2} \;, \tag{2.45}$$

where $\phi_n(\xi) = (1-\xi)^{n/3} + (1+\xi)^{n/3}$. And for the exchange potential energy per particle in the Coulomb case

$$e_p^x = -\left(\frac{2}{3\pi^5}\right)^{1/3} \frac{9\pi}{8}\phi_4(\xi)\frac{1}{r_s} \;, \tag{2.46}$$

which follows from Eq. (2.42) and Eqs. (D2)-(D3). The expression for finite μ can be found in Ref. (Paziani *et al.*, 2006) (see their Eqs. (15)-(16)).

3. Definition of the static structure factor

If we introduce the microscopic spin dependent number density

$$\rho_\sigma(\mathbf{r}) = \sum_{i=1}^{N} \delta_{\sigma,\sigma_i}\delta(\mathbf{r} - \mathbf{r}_i) \;, \tag{2.47}$$

and its Fourier transform $\rho_{\mathbf{k},\sigma}$, then the spin-resolved static structure factors are defined as $S_{\sigma,\sigma'}(\mathbf{k}) = \langle \rho_{\mathbf{k},\sigma}\rho_{-\mathbf{k},\sigma'}\rangle/N$, which, for the homogeneous and isotropic fluid, can be rewritten as

$$S_{\sigma,\sigma'}(k) = \frac{n_\sigma}{n}\delta_{\sigma,\sigma'} + \frac{n_\sigma n_{\sigma'}}{n}\int [g_{\sigma,\sigma'}(r) - 1]e^{-i\mathbf{k}\cdot\mathbf{r}}\, d\mathbf{r} + \frac{n_\sigma n_{\sigma'}}{n}(2\pi)^3\delta(\mathbf{k}) \;, \tag{2.48}$$

From now on we will ignore the delta function at $\mathbf{k} = 0$. The total (spin-summed) static structure factor is $S = \sum_{\sigma,\sigma'} S_{\sigma,\sigma'}$. Due to the charge sum rule (2.39) we must have $\lim_{k\to 0} S(k) = 0$. In Sec. E.2 we will show that the small k behavior of $S(k)$ has to start from the term of order k^2.

E. Results for the radial distribution function and structure factor

The radial distribution function and structure factor have been calculated through DMC by Ortiz and Ballone (Ortiz and Ballone, 1994). In Fig. 1 we show their results for the radial distribution function and in Fig. 2 their results for the structure factor.

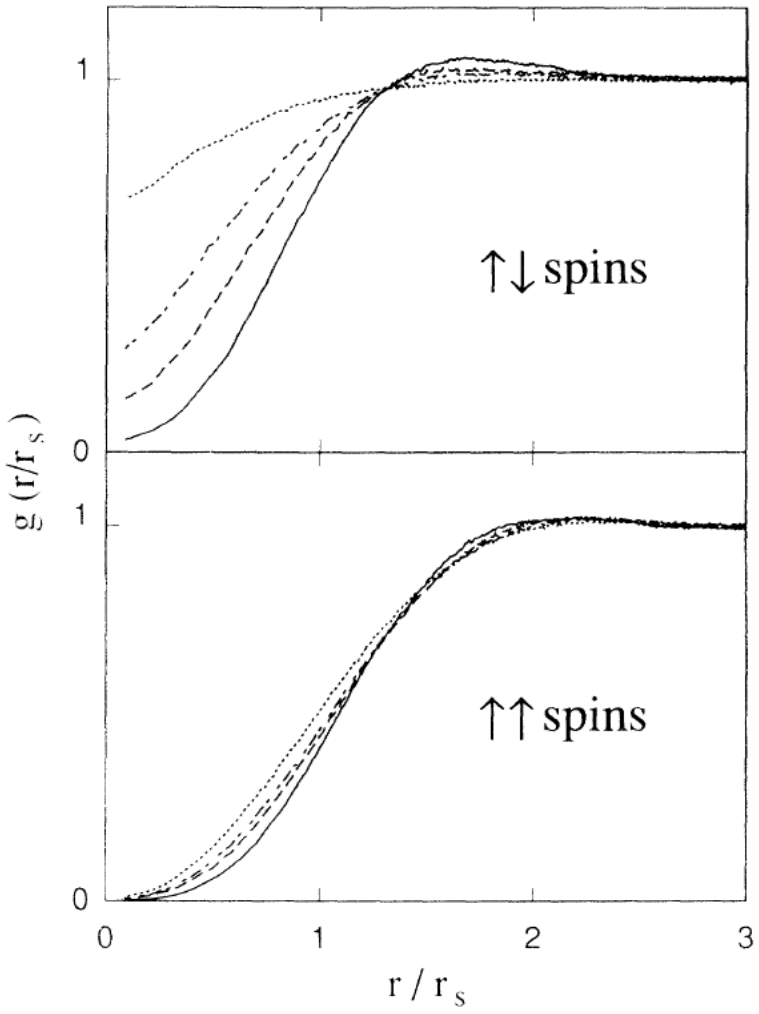

FIG. 1 Radial distribution function $g(r)$ computed by DMC method (mixed estimator) for the unpolarized $\xi = 0$ case and the fully polarized $\xi = 1$ case. $r_s = 1$ (dotted line), $r_s = 3$ (dash-dotted line), $r_s = 5$ (dashed line), and $r_s = 10$ (full line). r is in units of a Bohr radius. (Figure reproduced here by courtesy of the authors of Ref. (Ortiz and Ballone, 1994))

F. Results for the internal energy

The behavior of the internal energy of the Jellium in its ground state has been determined through DMC by Ceperley and Alder (Ceperley and Alder, 1980). Their result is shown in Fig. 3. Three phases of the fluid appeared, for $r_s < 75$ the stable phase is the one of the unpolarized Jellium, for $75 < r_s < 100$ the one of the polarized fluid, and for $r_s > 100$ the one of the Wigner crystal. The Wigner formula of Eq. (D11) turns out to be a rather good approximation. They used systems from $N = 38$ to $N = 246$ electrons.

III. JELLIUM AT FINITE TEMPERATURE

For the Jellium at finite temperature it is convenient to introduce the *electron degeneracy parameter* $\Theta = T/T_F$, where T_F is the Fermi temperature

$$T_F = T_D \frac{(2\pi)^2}{2[(2-\xi)\alpha_3]^{2/3}}, \tag{3.1}$$

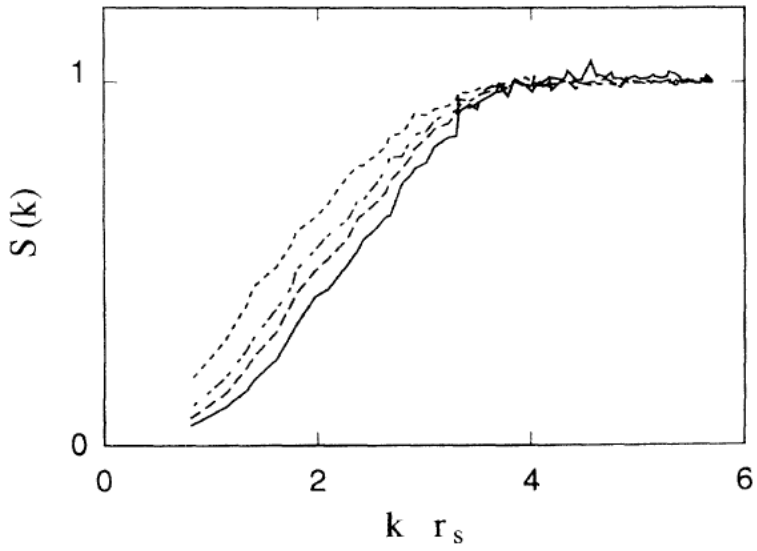

FIG. 2 Structure factor $S(k)$ computed by the DMC method (mixed estimator). The r_s considered and the symbols are the same as those of Fig. 1. (Figure reproduced here by courtesy of the authors of Ref. (Ortiz and Ballone, 1994))

here ξ is the polarization of the fluid that can be either $\xi = 0$, for the unpolarized case, and $\xi = 1$, for the fully polarized case, $\alpha_3 = 4\pi/3$, and

$$T_D = \frac{n^{2/3}\hbar^2}{mk_B}, \tag{3.2}$$

is the degeneracy temperature, for temperatures higher than T_D quantum effects are less relevant.

The state of the fluid will then depend also upon the *Coulomb coupling parameter*, $\Gamma = e^2/r_s a_0 k_B T$ (Brown *et al.*, 2013).

A. Monte Carlo simulation (Path Integral)

The *density matrix* of a many-fermion system at temperature $k_B T = \beta^{-1}$ can be written as an integral over all paths $\{R_t\}$

$$\rho_F(R_\beta, R_0; \beta) = \frac{1}{N!}\sum_{\mathcal{P}}(-1)^{\mathcal{P}} \oint_{\mathcal{P}R_0 \to R_\beta} dR_t \, \exp(-S[R_t]). \tag{3.3}$$

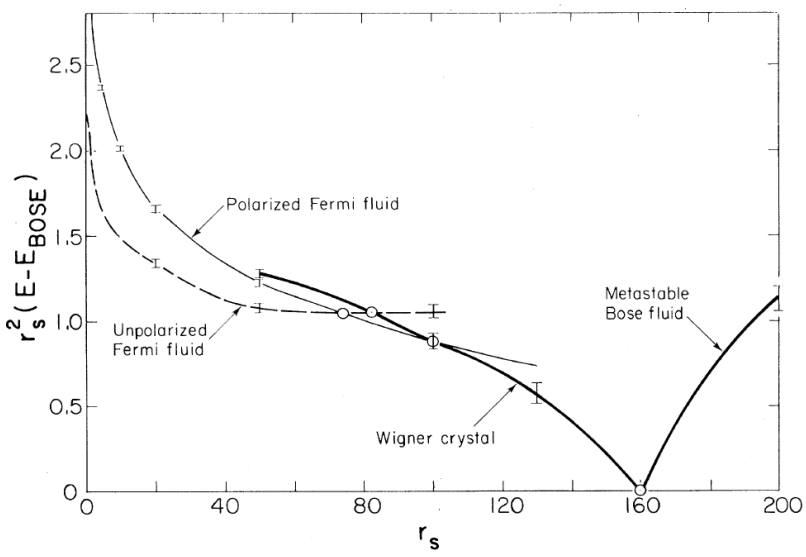

FIG. 3 The energy of the four phases studied relative to that of the lowest boson state times r_s^2 in Rydbergs as a function of r_s in Bohr radii. The boson system undergoes Wigner crystallization at $r_s = 160 \pm 10$. The fermion system has two phase transitions, crystallization at $r_s = 100 \pm 20$ and depolarization at $r_s = 75 \pm 5$. (Figure reproduced here by courtesy of the authors of Ref. (Ceperley and Alder, 1980))

the path $R(t)$ begins at $\mathcal{P}R_0$ and ends at R_β and $\mathcal{P}$ is a permutation of particles labels. For nonrelativistic particles interacting with a potential $V(R)$ the *action* of the path, $S[R_t]$, is given by (see appendix F)

$$S[R_t] = \int_0^\beta dt \left[\frac{r_s^2}{4} \left| \frac{dR(t)}{dt} \right|^2 + V(R_t) \right]. \tag{3.4}$$

Thermodynamic properties, such as the energy, are related to the diagonal part of the density matrix, so that the path returns to its starting place or to a permutation $\mathcal{P}$ after a time β.

To perform Monte Carlo calculations of the integrand, one makes imaginary time discrete, so that one has a finite (and hopefully small) number of time slices and thus a classical system of N particles in M time slices; an equivalent NM particle classical system of "polymers" (Ceperley, 1995).

Note that in addition to sampling the path, the permutation is also sampled. This is equivalent to allowing the ring polymers to connect in different ways. This macroscopic "percolation" of the polymers is directly related to superfluidity as Feynman (Feynman, 1953a,b,c) first showed. Any permutation can be broken into cycles. Superfluid behavior can occur at low temperature when the probability of exchange cycles on the order of the system size is non-negligible. The *superfluid fraction* can be computed in a path integral Monte Carlo calculation as described in Ref. (Pollock and Ceperley, 1987). The same method could be used to calculate the *superconducting fraction* in Jellium at low temperature. However, the straightforward application of those techniques to Fermi systems means that odd permutations subtract from the integrand. This is the "fermion sign problem" (Ceperley, 1991) which will be discussed in the next section.

Thermodynamic properties are averages over the thermal $N-$fermion density matrix which is defined as a thermal occupation of the exact eigenstates $\phi_i(R)$

$$\rho_F(R, R'; \beta) = \sum_i \phi_i^*(R) e^{-\beta E_i} \phi_i(R'). \tag{3.5}$$

The partition function is the trace of the density matrix

$$Z(\beta) = e^{-\beta F} = \int dR\, \rho_F(R, R; \beta) = \sum_i e^{-\beta E_i}. \tag{3.6}$$

Other thermodynamic averages are obtained as

$$\langle \mathcal{O} \rangle = Z(\beta)^{-1} \int dR dR' \, \langle R|\mathcal{O}|R'\rangle \rho(R', R; \beta). \tag{3.7}$$

Note that for any density matrix the diagonal part is always positive

$$\rho(R, R; \beta) \geq 0, \tag{3.8}$$

so that $Z^{-1}\rho(R, R; \beta)$ is a proper probability distribution. It is the diagonal part which we need for many observables, so that probabilistic ways of calculating those observables are, in principle, possible.

Path integrals are constructed using the product property of density matrices

$$\rho(R_2, R_0; \beta_1 + \beta_2) = \int dR_1 \, \rho(R_2, R_1; \beta_2)\rho(R_1, R_0; \beta_1), \tag{3.9}$$

which holds for any sort of density matrix. If the product property is used M times we can relate the density matrix at a temperature β^{-1} to the density matrix at a temperature $M\beta^{-1}$. The sequence of intermediate points $\{R_1, R_2, \ldots, R_{M-1}\}$ is the path, and the *time step* is $\tau = \beta/M$. As the time step gets sufficiently small the Trotter theorem tells us that we can assume that the kinetic $\mathcal{T}$ and potential $\mathcal{V}$ operator commute so that: $e^{-\tau\mathcal{H}} = e^{-\tau\mathcal{T}}e^{-\tau\mathcal{V}}$ and the *primitive approximation* for the Boltzmannon density matrix is found (Ceperley, 1995). The Feynman-Kac formula for the Boltzmannon density matrix results from taking the limit $M \to \infty$. The price we have to pay for having an explicit expression for the density matrix is additional integrations; all together $3N(M-1)$. Without techniques for multidimensional integration, nothing would have been gained by expanding the density matrix into a path. Fortunately, simulation methods can accurately treat such integrands. It is feasible to make M rather large, say in the hundreds or thousands, and thereby systematically reduce the time-step error.

In addition to the internal energy and the static structure of the Jellium one could also measure its dynamic structure, the "superconducting fraction", the specific heat, and the pressure (Ceperley, 1995).

1. The direct path integral method

In the *direct fermion method* one sums over permutations just as bosonic systems. Odd permutations then contribute with a negative weight. The direct method has a major problem because of the cancellation of positive and negative permutations. This was first noted by Feynman and Hibbs (Feynman and Hibbs, 1965) who after describing the path integral theory for boson superfluid ^{4}He, noted: "The [path integral] expression for Fermi particles, such as ^{3}He, is also easily written down. However in the case of liquid ^{3}He, the effect of the potential is very hard to evaluate quantitatively in an accurate manner. The reason for this is that the contribution of a cycle to the sum over permutations is either positive or negative depending whether the cycle has an odd or an even number of atoms in its length L. At very low temperature, the contributions of cycles such as $L = 51$ and $L = 52$ are very nearly equal but opposite in sign, and therefore they very nearly cancel. It is necessary to compute the difference between such terms, and this requires very careful calculation of each term separately. It is very difficult to sum an alternating series of large terms which are decreasing slowly in magnitude when a precise analytic formula for each term is not available.

Progress could be made in this problem if it were possible to arrange the mathematics describing a Fermi system in a way that corresponds to a sum of positive terms. Some such schemes have been tried, but the resulting terms appear to be much too hard to evaluate even qualitatively.

[...]

The [explanation] of the superconducting state was first answered in a convincing way by Bardeen, Cooper, and Schrieffer. The path integral approach played no part in their analysis and *in fact has never proved useful for degenerate Fermi systems. [D. M. Ceperley italics]*"

When we measure a property $\mathcal{O}$ in a Monte Carlo calculation (Ceperley, 1991, 1996)

$$\langle \mathcal{O} \rangle = \frac{\int \Pi \mathcal{O}}{\int \Pi} \, , \tag{3.10}$$

where π is a function with both positive and negative pieces and the integrals are not only over coordinates but a sum over permutations is also tacitly assumed.

One introduces the distribution function for the importance sampling P

$$\langle \mathcal{O} \rangle = \frac{\int P[\Pi \mathcal{O}/P]}{\int P[\Pi/P]} \, , \tag{3.11}$$

and calculates

$$\langle \mathcal{O} \rangle = \frac{\sum_i \omega_i \mathcal{O}_i}{\sum_i \omega_i} \, , \tag{3.12}$$

where $\omega_i = \Pi_i/P_i$ and the sums are over M points distributed according to P. Then the variance of the measure is

$$\begin{aligned}
\sigma^2_{\mathcal{O}} &= \left\langle \left(\frac{\sum_i \omega_i \mathcal{O}_i}{\sum_i \omega_i} - \langle \mathcal{O} \rangle \right)^2 \right\rangle_P \\
&= \frac{1}{\left(\sum_i \omega_i\right)^2} \left\langle \left[\sum_i \omega_i (\mathcal{O}_i - \langle \mathcal{O} \rangle) \right]^2 \right\rangle_P \\
&\approx \frac{1}{\left(\sum_i \omega_i\right)^2} \left\langle \sum_i \omega_i^2 (\mathcal{O}_i - \langle \mathcal{O} \rangle)^2 \right\rangle_P \\
&= \frac{1}{M \left(\int \Pi\right)^2} \left\langle \omega^2 (\mathcal{O} - \langle \mathcal{O} \rangle)^2 \right\rangle_P \\
&= \frac{1}{M \left(\int \Pi\right)^2} \int \frac{\Pi^2 (\mathcal{O} - \langle \mathcal{O} \rangle)^2}{P} \ ,
\end{aligned} \tag{3.13}$$

where we assumed that the sampled points were uncorrelated. Choosing $P = q^2/\int q^2$ and solving $\delta\sigma^2_{\mathcal{O}}/\delta q = 0$ we find as the optimal distribution

$$P^* \propto |\Pi(\mathcal{O} - \langle \mathcal{O} \rangle)| \ . \tag{3.14}$$

The usually one chooses $P = |\Pi|/\int |\Pi|$. For bosons there are no problems since Π is everywhere positive, but for fermions one finds

$$\sigma^2_F = \sigma^2_B/\xi \ , \tag{3.15}$$

where the efficiency is

$$\xi = \left[\frac{\int \Pi}{\int |\Pi|} \right]^2 = \left[\frac{M_+ - M_-}{M} \right]^2 = \left[\frac{\Theta_F}{\Theta_B} \right]^2 = e^{-2\beta(\Omega_F - \Omega_B)} \ . \tag{3.16}$$

The average time that the simulation spend in the positive region of P is M_+/M and M_-/M is the average time spent in the negative region. The efficiency for the fermionic case is proportional to the square of the average sign: the positive sampled points in excess over the negative ones. From the expressions for the grand-thermodynamic potentials for the ideal Bose, Ω_B, and Fermi, Ω_F, gas we find for example

$$\xi = \begin{cases} e^{-N\rho^3\Lambda^3/(\sqrt{2}g)} & z \to 0 \\ e^{-N\rho 2g(b_{5/2}(1) - f_{5/2}(1))/\Lambda^3} & z \to 1 \end{cases} \ , \tag{3.17}$$

where $b_{5/2}(1) - f_{5/2}(1) \approx 0.4743$. We then see that for any z the efficiency becomes exponentially small in the number of particles. Moreover for a fixed N we find $\xi = e^{-2\beta(F_F - F_B)}$, with F_B the Helmholtz free energy of the Bose gas and F_F the one of the Fermi gas, and in the high temperature limit we find (Landau and Lifshitz, 1951)

$$\xi \approx e^{-2\rho N (2\pi\lambda\beta)^{3/2}/g}. \tag{3.18}$$

Whereas in the low temperature limit

$$F_F = F^0_F - \frac{1}{4\lambda} \frac{N}{\beta^2} \left(\frac{\pi}{3\rho} \right)^{2/3} \ , \tag{3.19}$$

$$F_B = -\frac{N}{\beta} \frac{b_{5/2}(1)}{b_{3/2}(1)} \left(\frac{T}{T_c} \right)^{3/2} \ , \tag{3.20}$$

where $T_c \simeq T_D 2\pi/(2.612g)^{2/3}$ is the Bose-Einstein condensation temperature, $F^0_F = N\epsilon_F + \Omega^0_F$ with $\epsilon_F = \mu$ the Fermi energy and $\Omega^0_F = -gV\epsilon_F^{5/2}/(15\pi^2\lambda^{3/2})$, and $N = gV(2m\epsilon_F)^{3/2}/6\pi^2\hbar^3$. So that in the limit $\beta \to \infty$ we find

$$\xi = e^{-2\beta F^0_F} \ , \tag{3.21}$$

with $F^0_F = g(1/6 - 1/15)V\epsilon_F^{5/2}/(\pi^2\lambda^{3/2}) > 0$, which shows how the efficiency of a direct Monte Carlo calculation on fermions becomes exponentially small as β and N increases. Exactly where the physics becomes more interesting.

The Fermion density matrix is defined (Ceperley, 1991, 1996) by the Bloch equation which describes its evolution in imaginary time

$$\frac{\partial}{\partial\beta}\rho_F(R,R_0;\beta) = -\mathcal{H}\rho_F(R,R_0;\beta), \tag{3.22}$$

$$\rho_F(R,R_0;0) = \mathcal{A}\delta(R-R_0), \tag{3.23}$$

where $\beta = 1/k_BT$ with T the absolute temperature and $\mathcal{A}$ is the operator of antisymmetrization. The *reach* of R_0, $\gamma(R_0,t)$, is the set of points $\{R_t\}$ for which

$$\rho_F(R_{t'},R_0;t') > 0 \quad 0 \le t' \le t, \tag{3.24}$$

where t is the imaginary thermal time. Note that

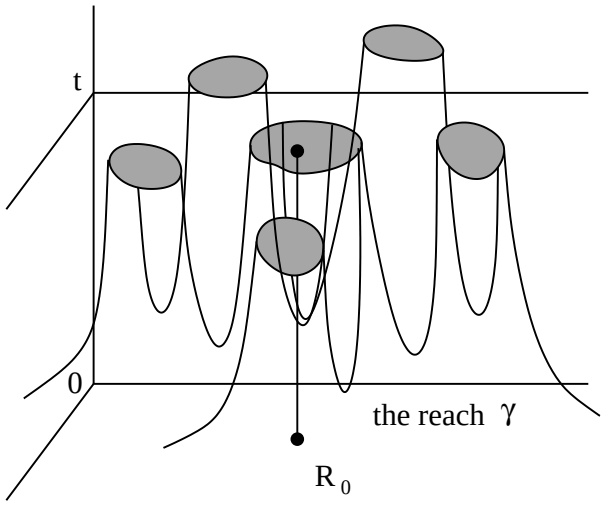

FIG. 4 Illustration of the reach $\gamma(R_0,t)$ of the fermion density matrix.

$$\rho_F(R_0,R_0;t) > 0, \tag{3.25}$$

and clearly

$$\rho_F(R,R_0;t)|_{R\in\partial\gamma(R_0,t)} = 0. \tag{3.26}$$

We want to show that (3.26) uniquely determines the solution. Suppose $\delta(R,t)$ satisfies the Bloch equation

$$\left(\mathcal{H} + \frac{\partial}{\partial t}\right)\delta(R,t) = 0, \tag{3.27}$$

in a space-time domain $\alpha = \{t_1 \le t \le t_1, R \in \Omega_t\}$. And the two conditions

$$\delta(R,t_1) = 0, \tag{3.28}$$

$$\delta(R,t)|_{R\in\partial\Omega_t} = 0 \quad t_1 \le t \le t_2, \tag{3.29}$$

are also satisfied. Consider

$$\int_{t_1}^{t_2} dt \int_{\Omega_t} dR\, e^{2V_0t}\delta(R,t)\left(\mathcal{H} + \frac{\partial}{\partial t}\right)\delta(R,t) = 0, \tag{3.30}$$

where V_0 is a lower bound for $V(R)$.

We have

$$\frac{\partial}{\partial t}\left[e^{2V_0t}\delta^2(R,t)\right] = 2V_0e^{2V_0t}\delta^2(R,t) + 2e^{2V_0t}\delta(R,t)\frac{\partial}{\partial t}\delta(R,t). \tag{3.31}$$

Since

$$\int_{t_1}^{t_2} dt \int_{\Omega_t} dR\, \frac{\partial}{\partial t}\left(\frac{e^{2V_0 t}}{2}\delta^2(R,t)\right) = \int_{t_1}^{t_2} dt\, \frac{\partial}{\partial t}\left(\frac{e^{2V_0 t}}{2}\int_{\Omega_t} dR\, \delta^2(R,t)\right) = \frac{e^{2V_0 t_2}}{2}\int_{\Omega_{t_2}} dR\, \delta^2(R,t_2), \tag{3.32}$$

where in the last equality we used Eq. (3.28). Then from Eq. (3.30) follows

$$\frac{e^{2V_0 t}}{2}\int_{\Omega_{t_2}} dR\, \delta^2(R,t_2) - e^{2V_0 t}\int_{t_1}^{t_2} dt \int_{\Omega_t} dR\, \left[V_0\delta^2(R,t) - \delta(R,t)\mathcal{H}\delta(R,t)\right] = 0. \tag{3.33}$$

Then using Eq. (3.29) we find

$$\frac{e^{2V_0 t}}{2}\int_{\Omega_{t_2}} dR\, \delta^2(R,t_2) + e^{2V_0 t}\int_{t_1}^{t_2} dt \int_{\Omega_t} dR\, \left[(V(R)-V_0)\delta^2(R,t) + \lambda\left(\boldsymbol{\nabla}\delta(R,t)\right)^2\right] = 0. \tag{3.34}$$

Each term in Eq. (3.34) is non-negative so it must be

$$\delta(R,t) = 0 \quad \text{in } \alpha. \tag{3.35}$$

Let ρ_1 and ρ_2 be two solutions of the restricted path problem and let $\delta = \rho_1 - \rho_2$. Then $\delta(R,t)|_{R\in\partial\gamma(R_0,t)} = 0$ for $t_1 \le t \le t_2$. By taking t_2 to infinity and t_1 to zero we conclude that the fermion density matrix is the unique solution.

Eq (3.34) also shows that the reach γ has the *tiling* property (Ceperley, 1991). Suppose it did not. Then there would exist a space-time domain with the density matrix non-zero inside and from which it is only possible to reach R_0 or any of its images $\mathcal{P}R_0$, with $\mathcal{P}$ any permutation of the particles, crossing the nodes of the density matrix. But such a domain cannot extend to $t = 0$ because in the classical limit there are no nodes. Then this density matrix satisfies for some $t_1 > 0$ the boundary conditions (3.28) and (3.29) and as a consequence it must vanish completely inside the domain contradicting the initial hypothesis.

We now derive the restricted path identity. Suppose ρ_F is the density matrix corresponding to some set of quantum numbers which is obtained by using the projection operator $\mathcal{A}$ on the distinguishable particle density matrix. Then it is a solution to the Bloch equation (3.22) with boundary condition (3.23). Thus we have proved the *Restricted Path Integral* identity

$$\rho_F(R_\beta, R_0; \beta) = \int dR'\, \rho_F(R', R_0; 0) \oint_{R'\to R_\beta \in \gamma(R_0)} dR_t\, e^{-S[R_t]}, \tag{3.36}$$

where the subscript means that we restrict the path integration to paths starting at R', ending at R_β and node-avoiding. The weight of the walk is $\rho_F(R', R_0; 0)$. It is clear that the contribution of all the paths for a single element of the density matrix will be of the same sign; positive if $\rho_F(R', R_0; 0) > 0$, negative otherwise.

Important in this argument is that the random walk is a continuous process so we can say definitely that if sign of the density matrix changed, it had to have crossed the nodes at some point.

The restricted path identity is one solution to Feynman's task of rearranging terms to keep only positive contributing paths for diagonal expectation values.

The problem we now face is that the unknown density matrix appears both on the left-hand side and on the right-hand side of Eq. (3.36) since it is used to define the criterion of node-avoiding paths. To apply the formula directly, we would somehow have to self-consistently determine the density matrix. In practice what we need to do is make an *ansatz*, which we call ρ_T, for the nodes of the density matrix needed for the restriction. The *trial density matrix*, ρ_T, is used to define trial nodal cells: $\gamma_T(R_0)$.

Then if we know the reach of the fermion density matrix we can use the Monte Carlo method to solve the fermion problem restricting the path integral (RPIMC) to the space-time domain where the density matrix has a definite sign (this can be done, for example, using a trial density matrix whose nodes approximate well the ones of the true density matrix) and then using the antisymmetrization operator to extend it to the whole configuration space. This will require the complicated task of sampling the permutation space of the $N-$particles (Ceperley, 1995). Recently it has been devised an intelligent method to perform this sampling through a new algorithm called the *worm* algorithm (Boninsegni *et al.*, 2006). In order to sample the path in coordinate space one generally uses various generalizations of the Metropolis rejection algorithm (Metropolis *et al.*, 1953) and the *bisection method* (Ceperley, 1995) in order to accomplish multislice moves which becomes necessary as τ decreases.

The *pair-product approximation* was used (Brown *et al.*, 2013) (see appendix G) to write the many-body density matrix as a product of high-temperature two-body density matrices (Ceperley, 1995). The pair Coulomb density matrix was determined using the results of Pollock (Pollock, 1988) even if these could be improved using the results

of Vieillefosse (Vieillefosse, 1994, 1995). This procedure comes with an error that scales as $\sim \tau^3/r_s^2$ where $\tau = \beta/M$ is the *time step*, with M the number of imaginary time discretizations. A more dominate form of time step error originates from paths which cross the nodal constraint in a time less than τ. To help alleviate this effect, Brown *et al.* (Brown *et al.*, 2013) use an image action to discourage paths from getting too close to nodes. Additional sources of error are the finite size one and the sampling error of the Monte Carlo algorithm itself. For the highest density points, statistical errors are an order of magnitude higher than time step errors.

The results at a given temperature T where obtained starting from the density matrix in the classical limit, at small thermal times, and using repetitively the *squaring* method

$$\rho_F(R_1, R_2; \beta) = \int dR' \, \rho_F(R_1, R'; \beta/2)\rho_F(R', R_2; \beta/2). \tag{3.37}$$

Time doubling is an improvement also because if we have accurate nodes down to a temperature T, we can do accurate simulations down to $T/2$. Eq. (3.37) is clearly symmetric in R_1 and R_2. The time doubling cannot be repeated without reintroducing the sign problem.

Brown *et al.* (Brown *et al.*, 2013) use $N = 33$ electrons for the fully spin polarized system and $N = 66$ electrons for the unpolarized system.

B. Results for the radial distribution function and structure factor

In the classical Debye-Hückel limit one has (Hansen, 1973; Hansen and McDonald, 1986)

$$g_{DH}(r) = \exp\left[-\frac{\Gamma}{r}\exp(-k_D r_s a_0 r)\right], \tag{3.38}$$

were $k_D = \sqrt{4\pi\beta n e^2}$. And for the structure factor, after linearizing Eq. (3.38) for $r \gg 1/k_D r_s a_0$,

$$S_{DH}(k) = \frac{k^2}{k^2 + 3\Gamma}. \tag{3.39}$$

A serious weakness of the linearized approximation is the fact that it allows $g(r)$ to become negative at small r. This failing is rectified in the non-linear version (3.38).

In the ground state the radial distribution function and structure factor have been calculated by Ortiz and Ballone (Ortiz and Ballone, 1994).

In Fig. 5 we present the RPIMC results of Brown *et al.* (Brown *et al.*, 2013).

C. Results for the internal energy

Given the total internal energy per particle of the fluid e_{tot}, the exchange and correlation energy per particle is

$$e_{xc}(T) = e_{tot}(T) - e_0(T). \tag{3.40}$$

where $e_0(T)$ is the kinetic energy of a free Fermi gas at temperature T. And

$$e_{xc}(T) = e_x(T) + e_c(T). \tag{3.41}$$

where $e_x(T)$ is the Hartree-Fock exchange energy for a Fermi gas at temperature T (see Eq. (7) of Ref. (Perdew and Zunger, 1981)).

For fixed polarizations $\xi = 0$, the unpolarized case, and for $\xi = 1$, the fully polarized case, one has

$$e_0 = (2-\xi)\frac{r_s^3}{3\pi\beta^{5/2}}\frac{1}{\mathrm{Ry}^{5/2}} I(3/2, \kappa), \tag{3.42}$$

$$e_x = -(2-\xi)\frac{r_s^3}{6\pi^2\beta^2}\frac{1}{\mathrm{Ry}^2}\int_0^\infty \frac{dx}{1+e^{x-\kappa}}\int_0^\infty \frac{dy}{1+e^{y-\kappa}}\int_{-1}^1 \frac{dz}{\sqrt{x/y}+\sqrt{y/x}-2z}, \tag{3.43}$$

where

$$I(\nu, \kappa) = \int_0^\infty \frac{x^\nu}{1+e^{x-\kappa}}\, dx, \tag{3.44}$$

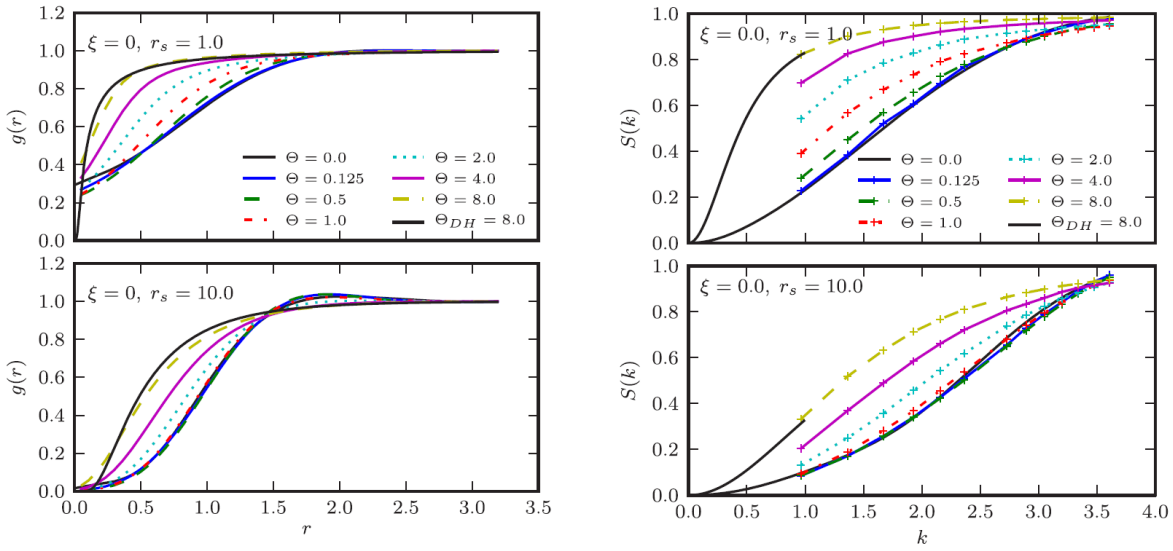

FIG. 5 Pair correlation functions (on the left) for $r_s = 1.0$ and $r_s = 10.0$ in the unpolarized state. Also shown is the small r part of the classical Debye-Hückel limit at $\Theta = 8.0$; see Eq. (3.38). The Debye-Hückel limit is not yet reached at $\Theta = 8.0$ for the lower density $r_s = 10.0$. Static structure factors (on the right) for $r_s = 1.0$ and $r_s = 10.0$ in the unpolarized state. Also shown is the small k part of the classical Debye-Hückel limit at $\Theta = 8.0$; see Eq. (3.39). (Figure reproduced here by courtesy of the authors of Ref. (Brown *et al.*, 2013))

and κ is determined from

$$I(1/2, \kappa) = \frac{2}{3}\Theta^{-3/2}. \tag{3.45}$$

For the expressions at an intermediate polarization $0 < \xi < 1$ see the appendix A. It is still missing an analysis of the finite temperature Jellium at intermediate polarizations. This would be important for a clearer determination of the Jellium phase diagram.

In Fig. 6 we present the RPIMC results of Brown *et al.* (Brown *et al.*, 2013).

In Ref. (Brown *et al.*, 2014) a comparison is given between these calculations to previous estimations of the Jellium correlation energy. Such parameterizations generally fall into two categories: those which extend down from the classical regime and those which assume some interpolation between the $T = 0$ and high-T regimes. From the former group, in Fig. 7, Brown *et al.* plot e_c coming from Debye-Hückel (DH) theory which solves for the Poisson-Boltzmann equations for the classical one-component plasma and the quantum corrections of Hansen *et al.* (Hansen, 1973; Hansen and Vieillefosse, 1975) of the Coulomb system both with Wigner-Kirkwood corrections (H+WK) and without (H). Clearly these methods do not perform well in the quantum regime below the Fermi temperature since they lack quantum exchange.

The Random Phase Approximation (RPA) (Gupta and Rajagopal, 1980; Perrot and Dharma-wardana, 1984) is a reasonable approximation in the low-density, high-temperature limit (where it reduces to DH) and the low-temperature, high-density limit, since these are both weakly interacting regimes. Its failure, however, is most apparent in its estimation of the equilibrium, radial distribution function $g(r)$ which becomes negative for stronger coupling. Extensions of the RPA into intermediate densities and temperatures have largely focused on constructing local-field corrections (LFC) through interpolation since diagrammatic resummation techniques often become intractable in strongly-coupled regimes. Singwi *et al.* (Singwi *et al.*, 1968) introduced one such strategy. Tanaka and Ichimaru (Tanaka and Ichimaru, 1986) (TI) extended this method to finite temperatures and provided the shown parameterization of the Jellium correlation energy. This method appear to perform marginally better than the RPA at all temperatures, though it still fails to produce a positive-definite $g(r)$ at values of $r_s > 2$. A third, more recent approach introduced by Perrot and Dharma-wardana (PDW) (Perrot and Dharma-wardana, 2000) relies on a classical mapping where the distribution functions of a classical system at temperature T_{cf}, solved for through the hypernetted-chain equation, reproduce those for the quantum system at temperature T. In a previous work, PDW showed such a temperature T_q existed for the classical system to reproduce the correlation energy of the quantum system at $T = 0$ (Dharma-wardana and Perrot, 2000). To extend this work to finite temperature quantum systems, they use the simple

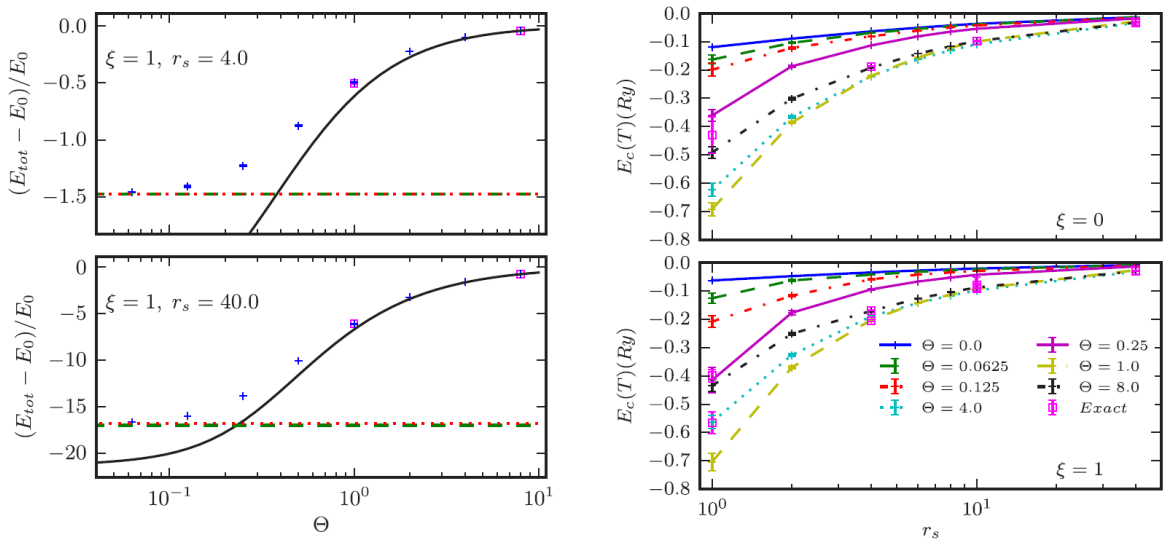

FIG. 6 Excess energies $E_{xc} = e_{xc}$ (on the left) for $r_s = 4.0$ and $r_s = 40.0$ for the polarized state ($E_0 = e_0$). For both densities the high temperature results fall smoothly on top of previous Monte Carlo energies for the classical electron gas (Pollock and Hansen, 1973) (solid line). Differences from the classical Coulomb gas occur for $\Theta < 2.0$ for $r_s = 4.0$ and $\Theta < 4.0$ for $r_s = 40.0$. Simulations with the Fermion sign (squares) confirm the fixed-node results at $\Theta = 1.0$ and 8.0. The zero-temperature limit (dotted line) smoothly extrapolates to the ground state QMC results of Ceperley-Alder (Ceperley and Alder, 1980) (dashed line). Correlation energy $E_c(T) = e_c(T)$ (on the right) of the 3D Jellium at several temperatures and densities for the unpolarized (top) and fully spin-polarized (bottom) states. Exact (signful) calculations (squares) confirm the fixed-node results where possible ($\Theta = 8.0$ for $\xi = 0$ and $\Theta = 4.0, 8.0$ for $\xi = 1$). (Figure reproduced here by courtesy of the authors of Ref. (Brown *et al.*, 2013))

interpolation formula $T_{cf} = \sqrt{T^2 + T_q^2}$. This interpolation is clearly valid in the low-T limit where Fermi liquid theory gives the quadratic dependence of the energy on T. Further in the high-T regime, T dominates over T_q as the system becomes increasingly classical. The PDW line in Fig. 7 clearly matches well with the RPIMC results in these two limits. It is not surprising, however, that in the intermediate temperature regime, where correlation effects are greatest, the quadratic interpolation fails. A contemporary, but similar approach by Dutta and Dufty (Dutta and Dufty, 2013) uses the same classical mapping as PDW which relies on matching the $T = 0$ pair correlation function instead of the correlation energy. While we expect this to give more accurate results near $T = 0$, we would still expect a breakdown of the assumed Fermi liquid behavior near the Fermi temperature. Future Jellium work will include creating a new parameterization of the correlation energy which uses the RPIMC data directly. In doing so, simulations at higher densities and both lower and higher temperatures may be necessary in order to complete the interpolation between the ground state and classical limits.

D. Phase diagram

The *worm-dense* regime for both the fully spin-polarized $\xi = 1$ and unpolarized $\xi = 0$ systems has been studied through RPIMC by Brown *et al.* (Brown *et al.*, 2013). This study complements the previous Monte Carlo studies on the classical one-component plasma (Pollock and Hansen, 1973) and the inclusion of first order quantum mechanical effects by Jancovici (Jancovici, 1978) and Hansen and Vieillefosse (Hansen and Vieillefosse, 1975). However, the accuracy of these results quickly deteriorates as the temperature is lowered and quantum correlations play a greater role (Jones and Ceperley, 1996). This breakdown is most apparent in the *warm-dense regime* where both Γ and Θ are close to unity as shown in Fig. 8.

In the RPIMC of Brown *et al.* (Brown *et al.*, 2013) the trial density matrix was taken as the free electron density matrix

$$\rho_T(R, R'; \tau) = (4\pi\tau/r_s^2)^{-3N/2} \mathcal{A} \exp\left[-\frac{(R - R')^2}{4\tau/r_s^2}\right], \tag{3.46}$$

where $\tau = \beta/M$ with M the number of imaginary time discretizations. This approximation should be best at high

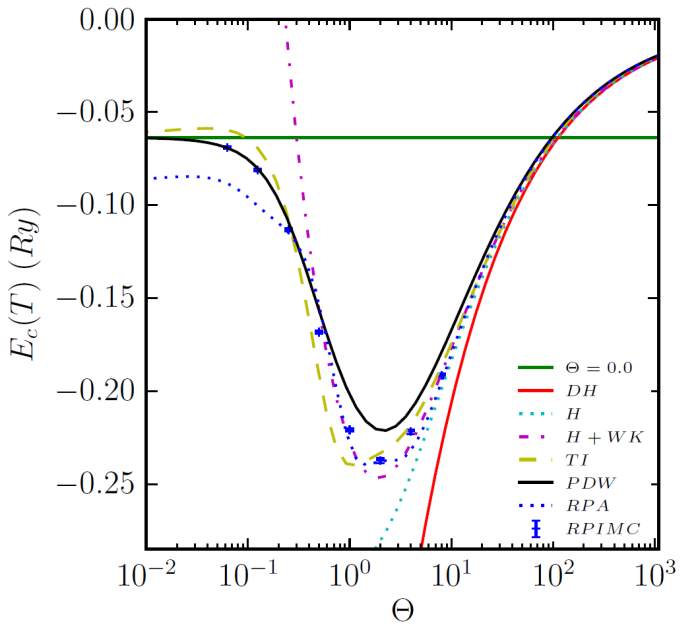

FIG. 7 Correlation energy $E_c(T) = e_c(T)$ of the Jellium at $r_s = 4.0$ for the unpolarized $\xi = 0$ state from the RPIMC calculations (RPIMC) and several previous parameterizations as a function of Θ. The latter include Debye-Hückel (DH), Hansen (H), Hansen+Wigner-Kirkwood (H+WK), Random Phase Approximation (RPA), Tanaka and Ichimaru (TI), and Perrot and Dharma-wardana (PDW). Also included is the ground state $\Theta = 0.0$ result for comparison. (Figure reproduced here by courtesy of the authors of Ref. (Brown *et al.*, 2014))

temperature and low density when correlation effects are weak. The free-particle nodal approximation performs well for the densities studied by Brown *et al.* (Brown *et al.*, 2013). Further investigation is needed at even smaller values of r_s and lower temperatures in order to determine precisely where this approximation begins to fail. Such studies will necessarily require algorithmic improvements, however, because of difficulty in sampling paths at low density and low temperature.

IV. SOME PHYSICAL REALIZATIONS AND PHENOMENOLOGY

The Jellium model is a system of pointwise electrons of charge e and number density n in the three dimensional Euclidean space filled with an uniform neutralizing background of charge density $-en$. The zero temperature, ground-sate, properties of the statistical mechanical system thus depends just on the electronic density n, or the Wigner-Seitz radius $r_s = (3/4\pi n)^{1/3}/a_0$ where a_0 is Bohr radius, or the Coulomb coupling parameter Γ.

The model can be used for example as a first approximation to describe free electrons in metallic elements (Ashcroft and Mermin, 1976) ($2 \lesssim r_s \lesssim 4$) or the interior of a white dwarf (Shapiro and Teukolsky, 1983) ($r_s \simeq 0.01$). More generally it is an essential ingredient for the study of ionic liquids (see Ref. (Hansen and McDonald, 1986) Chapter 10 and 11): *molten-salts*, *liquid-metals*, and *ionic-solutions*. In molten alkali halides the masses of the cation and the anion are comparable whereas in liquid metals the anions are replaced by electrons from the valence or conduction bands. The very small mass of the electron leads to a pronounced disymmetry between the two species present in the metal. In particular, whereas the behavior of the cations can be discussed in the framework of classical statistical mechanics, the electron form a degenerate Fermi gas for which a quantum-mechanical treatment is required. Restricting to the class of simple metals in which the electronic valence states are well separated in energy from the tightly-bound core states; their properties are reasonably well described by the nearly-free-electron model. Metals that are classified in this sense include the alkali metals, magnesium, zinc, mercury, gallium, and alluminium. Other liquid metals (noble and transition metals, alkaline earths, lanthanides, and actinides) have more complicated electronic structures, and the theory of such systems is correspondingly less well advanced. Molten-salt solutions are mixtures of liquid metals and molten salts. Ionic-solutions are liquids consisting of a solvent formed by neutral, polar molecules, and a solute that dissociates into positive and negative ions. They vary widely in complexity: in the classic

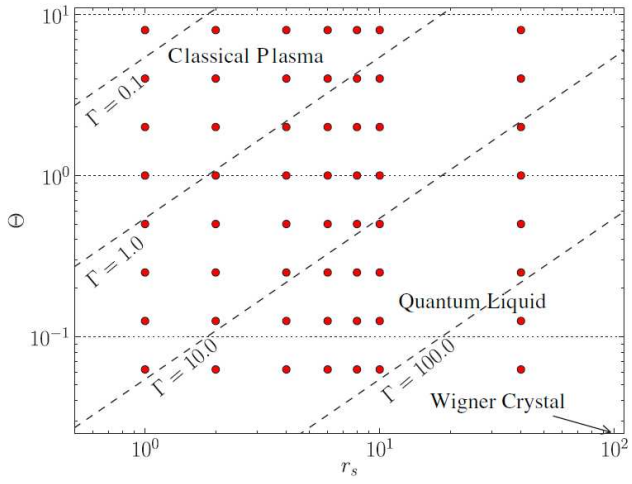

FIG. 8 Temperature-density phase diagram showing the points considered in Ref. (Brown *et al.*, 2013). Several values of the Coulomb coupling parameter Γ (dashed lines) and the electron degeneracy parameter Θ (dotted lines) are also shown. (Figure reproduced here by courtesy of the authors of Ref. (Brown *et al.*, 2013))

electrolyte solutions, the cations and anions are comparable in size and absolute charge, whereas macromolecular ionic solutions contain both macroions (charged polymers chains or coils, micelles, charged colloidal particles, etc.) and microscopic counterions.

Experimentally, Wigner crystallization was first unambiguously observed to occur in a quasi-classical, quasi-two-dimensional fluid of electrons floating on top of liquid ^{4}He substrate (Grimes and Adams, 1979). Such quasi-two-dimensional electron systems are currently realized in the laboratory in various semiconductors structures, but is has proven difficult to reach the very low temperatures needed for Wigner crystallization of electrons in the quantal regime without losing their collective behavior through the unavoidable presence of impurities. Furthermore, the application of a strong magnetic field to a quasi-two-dimensional electron fluid in semiconductor structures provides a very effective way to squeeze out the translational kinetic energy without going to very low densities. The Wigner crystallization in the exactly-two-dimensional Jellium has been found by DMC calculations to be past $r_s = 37 \pm 5$ (Tanatar and Ceperley, 1989).

Whereas the finite temperature properties of Jellium depends additionally on the electron degeneracy parameter Θ. Apart from its purely speculative interest, the temperature dependence of the Jellium properties are certainly of great astrophysical relevance. Examples are dense plasmas in the interior of giant planets (Knudson, 2012) and brown dwarfs atmospheres. Other uses could be in highly compressed laboratory plasmas, such as laser plasmas (Ernstorfer, 2009), inertial confinement fusion plasmas (Fletcher, 2014), and pressure-induced modifications of solids, such as insulator-metal transitions (Mazzola *et al.*, 2014). These examples justify the growing interest recently emerged in matter under extreme conditions in the warm-dense regime (Dornheim *et al.*, 2016).

It would be desirable to perform a full quantum Monte Carlo simulation for the Restricted Primitive Model (RPM), an electrically neutral fluid of particles of opposite charge made thermodynamically stable by preventing the particles collapse through the inclusion of a hard core of a certain radius centered on each particle. Some attempts have been made for large mass asymmetries between the positive and negative charges requiring a mixed MC (classical) - DMC (quantum) treatment (Ceperley *et al.*, 2002; Dewing and Ceperley, 2002) where one treats the slow ions through the Born-Oppenheimer approximation and the fast ones at zero temperature. Other alternatives could be a mixed MC - PIMC or more generally a full PIMC one.

Follows an excerpt from the last March and Tosi book (March and Tosi, 2002).

A. Molten halides and some alloys of metallic elements

Unlike monatomic fluid like liquid argon already for liquid sodium it is necessary to view it as formed of positive ions and conduction electrons. More obviously, one has to start from an ionic picture in describing a sodium chloride melt or liquid lithium iodide.

The crystal structures of halide compounds arise from electronic charge transfer and local compensation of positive and negative ionic charges through chemical order. Nature achieves charge compensation in two qualitatively distinct ways. The first involves halogen sharing and high coordination for the metal ions, as for example in alkali, alkaline-earth and lanthanide metal halides. In the second type charge compensation takes place within well defined molecular units, either monomeric ones as for example in $HgC1_2$ and $SbC1_3$ or dimeric ones as in $A1Br_3$.

Neutron diffraction studies of metal halide melts have shown that melting usually preserves the type of chemical order found in the crystal. For example, the melting of $MgC1_2$ or $YC1_3$ can be viewed as a transition from an ionic crystal to an ionic liquid (ionic-to-ionic, in short) and that of $SbC1_3$ or $A1Br_3$ as a molecular-to-molecular transition. However, $A1Br_3$ and $FeC1_3$ are known instances of ionic-to-molecular melting. Intermediate-range order (IRO), extending over distances of 5 to 10 Å say, has been revealed in both network-type and molecular-type melts. This type of order is well known in glassy materials.

1. Alkali halide vapours

Even for alkali halides, the vapour at coexistence with the hot melt is made of molecular monomers and dimers. The same basic ionic model can account for cohesion in these molecules as in the solid and dense liquid states, provided that distortions of the electron shells of the ions from electrical and overlap effects are accounted for.

2. Coulomb ordering in monohalides and dihalides

3. Alkali halides

The nature of Coulomb ordering in a molten salt like NaCl is such that the distribution of the screening charge density around any given ion oscillates in space, rather than being a monotonic function of distance as in the Debye-Hückel theory. Nevertheless, a meaningful definition of screening length in a dense ionic fluid can be based on the Debye-Hückel concept of the potential drop across the dipole layer formed by an ion and by the screening charge distribution.

4. Noble-metal halides

The monovalent Cu^+ and Ag^+ ions, with an outer shell of ten *d*-electrons, have small ionic radius and large electronic polarisability in comparison with the corresponding alkali ions. These properties lead to some hybridisation and covalent binding in copper and silver halides, tending to favor low coordination of first neighbors and promoting remarkable transport behaviors.

The ionic conductivity of solid CuBr and CuI increases rapidly with temperature, already reaching values of $\approx 0.1\ \Omega^{-1}\mathrm{cm}^{-1}$ before attaining, through two structural phase transitions, fast-ion (superionic) behavior of the Cu^+ ions before melting. A phase transition is also exhibited by AgI at 147 °C and is accompanied by a jump in ionic conductivity to a values of $\approx 1\ \Omega^{-1}\mathrm{cm}^{-1}$, typical of ionic melts. The Ag^+ ions in the a phase are disordered over many interstitial sites. Solid CuC1, AgC1 and AgBr also show premelting phenomena, with the ionic conductivity rising to values of $0.1 - 0.5\ \Omega^{-1}\mathrm{cm}^{-1}$.

These materials melt at relatively low temperature with a relatively low entropy change, while the ionic conductivity of the melt is comparable to that of molten alkali halides. Excess entropy has been released in the crystal before melting through the massive disordering of the metal ions. Diffraction data are available for all melts of this family: overall, their liquid structure can be described in term of a random close-packing of halogens, accommodating the metal ions in tetrahedral-like coordinations.

5. Fluorite-type superionic conductors

Fluorite-type materials such as SrC12 undergo a diffuse transition to a high-conductivity state before melting. The ionic conductivity and the entropy increase rapidly but continuously with temperature across the transition, whereas the heat capacity shows a peak. A high dynamic concentration of anionic Frenkel defects (interstitial-vacancy pairs) is gradually created across the transition, as revealed by neutron diffraction and diffuse quasi-elastic scattering studies on a variety of materials including $SrC1_2$, CaF_2, PbF_2 and UO_2. In other materials, such as $BaC1_2$ and $SrBr_2$, a superionic state is attained through a structural phase transition to the fluorite structure.

The liquid structure of $BaC1_2$ and $SrC1_2$ has been determined by neutron diffraction using isotopic substitution. In both melts, within the frame of the divalent cations, the halogen ion component is more weakly ordered. The liquid structure thus shows a remnant of the fast-ion conducting state that the solid attains through an extensive disordering of the anions.

The observed short-range ordering in molten $SrC1_2$ and $BaC1_2$ suggests that freezing may be viewed as a process in which the cationic component is independently crystallising and at the same time modulating the anions into the lattice periodicity. The anionic component in the hot crystal near melting may thus be described as a modulated "lattice liquid". In turn, the diffuse transition from the superionic to the "normal" state on cooling the $SrC1_2$ crystal may be viewed as a continuous process of anionic freezing inside the periodic force field of the metal-ion lattice.

6. Tetrahedral-network structure in $ZnCl_2$

The pair structure is also experimentally known for a number of other dihalide melts. The evolution of the liquid structure with increasing covalency versus ionicity of the bonding brings it from a cation-dominated structure to one in which the anions provide a "deformable frame" accommodating the doubly-charged cations. The $C1^-$-$C1^-$ structural correlations are not especially affected: the C1-C1 bond length stays in the range 3.6 to 3.8 Å.

The state of pronounced IRO in molten ZnC12 arises from strongly stable local tetrahedral structures through the formation of a network of chlorines. The partial distribution functions can be interpreted as describing a disordered close-packed arrangement of chlorine ions which provides tetrahedral sites for the Zinc ions. Such a structural arrangement is very similar to that of the glassy state of $ZnC1_2$: the Zn-C1 bond length is practically the same in the two states and the average coordination number of Zn is reported as 3.8 in the glass and ≈ 4 in the melt.

B. Structure of trivalent-metal halides

Two main trends emerge from liquid structure studies on trichlorides: (i) the trend from cation-dominated Coulomb ordering to loose octahedral-network structures across the series of lanthanide compounds including $YC1_3$, and (ii) the stabilization of molecular structures with strong intermolecular correlations leading to IRO. The overall structural evolution is governed by the increasing weight of covalency versus ionicity.

1. Octahedral-network formation in lanthanide chlorides

X-ray diffraction data on the series of molten rare-earth trichlorides show similar structural characters. The d_{MCl} bond length lies in the range 2.7-2.9 Å while the second-neighbor bond lengths are $d_{MM} \approx 5$ Å and $d_{ClCl} \approx 4$ Å, indicating a Coulomb ordering primarily ruled by the repulsion between the cations as discussed earlier for SrC12. Ionic conductivity and Raman scattering data suggest that the coordination of the metal ions is becoming more stable through the series, leading to a liquid structure which resembles a loose network of Cl-sharing octahedra.

2. Ionic-to-molecular melting in $AlCl_3$ and $FeCl_3$

YCl_3 is structurally isomorphous to $A1C1_3$ in the crystal phase. The octahedral coordination of the Y, Al and Fe ions in the crystal is apparent, which is basically preserved in $YC1_3$ on melting. The upper cluster illustrates the cooperative mechanism of metal-ion displacements by which the $A1_2C1_6$ and Fe_2Cl_6 molecules can form on melting, each dimer being in the shape of two tetrahedra sharing an edge. In $A1Br_3$ such an arrangement of A1 ions in tetrahedral sites already exists in the crystal. The melting of $A1C1_3$ and $FeCl_3$ also involves expansion of the chlorine packing.

3. Liquid haloaluminates

In $A1Cl_3$ and $A1Br_3$, while the pure melt is a molecular liquid, molten-salt behavior emerges on mixing with alkali halides. Complex anions are formed with the alkalis playing the role of counterions. Thus, starting from neutral $A1_2C1_6$ dimers in the $A1C1_3$ liquid, the $(A1_2C1_7)^-$ anion in the shape of two tetrahedra sharing a corner has been identified in mixtures with alkali chlorides. This anion is ultimately replaced by $(A1C1_4)^-$ anions at 1 : 1 stoichiometry.

The fluoroaluminates behave quite differently. The Na_3A1F_4 compound, known as cryolite, presents special interest because of its role in the industrial HaI1-Héroult process for the electrodeposition of A1 metal from alumina. The Raman spectra of molten $(A1F_3)_c$. $(NaF)_{l-c}$ and other Al-alkali fluoride mixtures give evidence for a gradual conversion of $(A1F_4)^-$ into $(A1Fs)^{2-}$ and $(A1F_6)^-$ as the solution becomes more basic with c decreasing below 0.5.

4. Molecular-to-molecular melting in $GaCl_3$ and $SbCl_3$

For other trihalides, such as $GaCl_3$ and $SbCl_3$ molecular units can be recognized as constituents in the crystal structure. Crystalline $GaC1_3$ can be viewed as composed of Ga_2C1_6 dimers. The crystal structure of $SbC1_3$ is instead built by packing chains of monomers in the shape of trigonal pyramids with metal ions at the apices. The stable molecular units in the vapour phase are the Ga_2C1_6 dimer and the $SbCl_3$ monomer.

The liquid structure of $SbCl_3$ at 80 °C has been studied by a combination of X-ray and neutron diffraction. It can be described as arising from separate monomeric units with strong intermolecular correlations. Each metal ion has three additional chlorine neighbors from other molecules: such a strongly distorted octahedral arrangement could result from stacking the monomers in chains like umbrellas, the dipole axes of molecules within a chain being strongly correlated over at least one or two molecular diameters.

The neutron diffraction patterns measured for molten $A1Br_3$, $GaBr_3$ and GaI_3 show three peaks at approximately 1.0, 1.9 and 3.4 $Å^{-1}$. The corresponding pair distribution functions exhibit a very well defined coordination shell of first neighbors, with coordination number 4.0 ± 0.2 for $A1Br_3$ and $GaBr_3$ and 3.75 ± 0.2 for GaI_3. The intermolecular correlations between halogens are quite significant, the corresponding coordination number being in the range typical of a random close-packing in the liquid state.

C. Chemical short-range order in liquid alloys

Fully ionized salts with a large band gap, like the alkali halides, remain ionic across melting. At the opposite extreme, melting of covalent semiconductors such as Ge and InSb involves a collapse of the covalent structure, which is directly revealed by an increase of coordination from 4 to values in the range 6-8 and by a sharp increase in electrical conductivity to an essentially metallic type. Between these extremes a number of systems have been identified which show a variety of intermediate electronic behavior in the liquid phase.

1. The CsAu compound

The stoichiometric CsAu compound crystallizes in the CsCl-type structure and is a strongly polar semiconductor with an optical band gap of 2.6 eV at room temperature. Its electrical conductivity drops on melting to a value which is comparable to molten salts. Electromigration experiments give evidence that Cs migrates to the cathode and Au to the anode, one Cs^+ and one Au^- being transported per elementary charge to the electrodes.

A neutron diffraction study of the liquid structure of the Cs-Au alloy shows a structure in the neutron structure factor at k = 1.2 $Å^{-1}$, which is interpreted as the "Coulomb prepeak" characteristic of chemical order. After Fourier transform of these data, the Cs-Au first neighbor distance at 3.6 Å can be followed up to 80% Cs, while the Cs-Cs distance at 5.3 Å characteristic of the pure Cs metal start emerging at 70% Cs.

2. Other alkali-based alloys with chemical short-range order

Interspecies ordering as shown by the Cs-Au system has been reported for a number of other alkali-based alloys, the alloying partners being elements of group III, IV or V. The formation of chemical short-range order at certain compositions is signalled by anomalies in electronic properties such as the electrical resistivity and the magnetic

susceptibility, which reflect a minimum in the electron density of states at the Fermi level if not the opening of a gap due to full charge transfer. Three different kinds of compound formation can be identified: (i) compound formation near the electronic octet composition A_4B as in Li-Pb or Li-Sn; (ii) compound formation near the equimolar composition AB, as in K-Pb or Rb-Pb; and (iii) compound formation near both these compositions, as in Li-Si, Li-Ge or Na-Sn. The data show increasing stability of the octet composition through the sequence Si, Ge, Sn and Pb, and decreasing stability through the sequence from Li to Cs.

A neutron diffraction measurement of the Bhatia-Thornton [6] concentration-structure factor in Li_4Pb has shown chemical order extending over a range of about 20 Å in the corresponding $g_{cc}(r)$ distribution function. With regard to alkali-group IV alloys in the second and third classes mentioned above, such as K-Pb or Na-Sn, it has proposed a model for order at equimolar composition which invokes formation of essentially tetrahedral Pb_4 or Sn_4 polyanions. Such tetrahedral "Zintl ions" are seen in the crystal structure of the equiatomic compound. In such a tetrahedral cluster the p-type electron states of Pb, say, would be split into bonding and antibonding states and the former could be filled by electron transfer from the alkali atoms.

The presence of polyanions in Zintl alloys also has dynamical consequences. A striking case is NaSn, in which the Sn_4 polyanions are observed to undergo jump reorientations and thereby to enhance the diffusivity of the Na cations by a paddle-wheel mechanism. These two types of disorder appear simultaneously as the melting point is approached.

D. Liquid metals

Some properties of simple liquid metals having conduction electrons in s and p states, that specifically reflect their nature as two-component liquids of ions and electrons are: (i) the effective interaction between pairs of ions as determined by screening of their bare Coulomb repulsions by the conduction electrons; (ii) the structural correlation functions involving the conduction electrons and supplementing the nuclear structure factor $S(k)$ in a full description of the liquid-metal structure; and (iii) the theory of electrical resistivity and viscosity of liquid metals. For a general account of liquid metals the book of March (March, 1990) may be consulted. in the limit when the effects of the ionic cores become negligible, we shall call the plasma particles "Jellium".

Appendix A: Ideal gas energy and exchange energy as a function of polarization

For the general case of N_+ spin-up particles the Fermi wave-vector for the spin-up (spin-down) particles will be

$$k_F^{\pm} = (1 \pm \xi)^{1/3} k_F, \tag{A1}$$

with

$$k_F = (3\pi^2 n)^{1/3} = (9\pi/4)^{1/3}/a_0 r_s, \tag{A2}$$

the Fermi wave-vector of the unpolarized fluid.

The Fermi energy will be

$$k_B T_F = \sum_\sigma \frac{(\hbar k_F^\sigma)^2}{2m} \tag{A3}$$

$$= \frac{\hbar^2 \left[(1+\xi)^{2/3} + (1-\xi)^{2/3}\right] k_F^2}{2m}. \tag{A4}$$

The degeneracy parameter will then be

$$\Theta = \frac{2m}{\hbar^2} \left(\frac{1}{3\pi^2 n}\right)^{2/3} \left(\frac{k_B T}{\left[(1+\xi)^{2/3} + (1-\xi)^{2/3}\right]}\right). \tag{A5}$$

Then finding κ^+ and κ^- from the following equations

$$I(1/2, \kappa^+) = \frac{2}{3}\Theta^{-3/2} \frac{(1+\xi)}{\left[(1+\xi)^{2/3} + (1-\xi)^{2/3}\right]^{3/2}}, \tag{A6}$$

$$I(1/2, \kappa^-) = \frac{2}{3}\Theta^{-3/2} \frac{(1-\xi)}{\left[(1+\xi)^{2/3} + (1-\xi)^{2/3}\right]^{3/2}}, \tag{A7}$$

---

[6] A. B. Bhatia and D. E. Thornton, *Phys. Rev. B* **2**, *3004 (1970)*

we can determine the kinetic energy per particle of the partially polarized, $0 < \xi < 1$, ideal Fermi gas

$$e_0 = \frac{2r_s^3}{3\pi\beta^{5/2}} \frac{1}{\mathrm{Ry}^{5/2}} \left[\frac{I(3/2,\kappa^+)}{(1+\xi)} + \frac{I(3/2,\kappa^-)}{(1-\xi)} \right] . \tag{A8}$$

The exchange energy on the other hand will be

$$e_x = -\frac{r_s^3}{3\pi^2\beta^2} \frac{1}{\mathrm{Ry}^2} \left[\frac{1}{(1+\xi)} \int_0^\infty \frac{dx}{1+e^{x-\kappa^+}} \int_0^\infty \frac{dy}{1+e^{y-\kappa^+}} \int_{-1}^1 \frac{dz}{\sqrt{x/y}+\sqrt{y/x}-2z} \right.$$
$$\left. + \frac{1}{(1-\xi)} \int_0^\infty \frac{dx}{1+e^{x-\kappa^-}} \int_0^\infty \frac{dy}{1+e^{y-\kappa^-}} \int_{-1}^1 \frac{dz}{\sqrt{x/y}+\sqrt{y/x}-2z} \right] , \tag{A9}$$

Appendix B: Jastrow, backflow, and three-body

In terms of the stochastic process governed by $f(R,t)$ one can write, using Kac theorem (Kac, 1951, 1959)

$$\int dR\, f(R,\tau) = \left\langle \exp\left[-\int_0^\tau dt\, E_L(R^t) \right] \right\rangle_{\mathrm{DRW}} , \tag{B1}$$

where $\langle \ldots \rangle_{\mathrm{DRW}}$ means averaging with respect to the diffusing and drifting random walk. Choosing a complete set of orthonormal wave-functions Ψ_i we can write for the true time dependent many-body wave-function

$$\phi(R,\tau) = \sum_i \Psi_i(R) \int dR' \Psi_i(R') \phi(R',\tau) \approx \Psi(R) \int dR\, f(R,\tau)$$
$$= \Psi(R) \left\langle \exp\left[-\int_0^\tau dt\, E_L(R^t) \right] \right\rangle_{\mathrm{DRW}} , \tag{B2}$$

where Ψ is the wave-function, of the set, of maximum overlap with the true ground-state, the trial wave-function. Assuming that at time zero we are already close to the stationary solution, for sufficiently small τ we can approximate

$$\left\langle \exp\left[-\int_0^\tau dt\, E_L(R^t) \right] \right\rangle_{\mathrm{DRW}} \approx e^{-\tau E_L(R^\tau)} . \tag{B3}$$

By antisymmetrising we get the Fermion wave-function

$$\phi_F(R,\tau) \approx \mathcal{A}\left[e^{-\tau E_L(R)} \Psi(R) \right] , \tag{B4}$$

where given a function $f(R)$ we define the operator (a symmetry of the Hamiltonian)

$$\mathcal{A}[f(R)] = \frac{1}{N_{\mathcal{P}}} \sum_{\mathcal{P}} (-1)^{\mathcal{P}} f(\mathcal{P}R) , \tag{B5}$$

here $N_{\mathcal{P}} = N_+!N_-!$ is the total number of allowed permutations $\mathcal{P}$.

This is called the local energy method to improve a trial wave-function. Suppose we start from a simple unsymmetrical product of single particle plane waves of N_+ spin-up particles with $k < k_F^+$ occupied and N_- spin-up particles with $k < k_F^-$ occupied, for the zeroth order trial wave-function. Equation (B4) will give us a first order wave-function of the Slater-Jastrow type (see equation (2.16)). If we start from an unsymmetrical Hartree-Jastrow trial wave-function the local energy with the Jastrow factor has the form

$$E_L = V - \lambda \sum_i \left[-k_i^2 - 2i\mathbf{k}_i \cdot \boldsymbol{\nabla}_i \sum_{j<k} u(r_{jk}) - \boldsymbol{\nabla}_i^2 \sum_{j<k} u(r_{jk}) + \left| \boldsymbol{\nabla}_i \sum_{j<k} u(r_{jk}) \right|^2 \right] , \tag{B6}$$

where $V = V(R)$ is the total potential energy and $r_{ij} = |\mathbf{r}_{ij}| = |\mathbf{r}_i - \mathbf{r}_j|$. Then the antisymmetrized second order wave-function has the form in Eq. (2.31), which includes backflow (see the third term), which is the correction inside the determinant and which affects the nodes, and three-body boson-like correlations (see last term) which do not affect the nodes.

Appendix C: The Random Phase Approximation

In this Appendix we will work on an unpolarized system.

Within the linear density response theory (Hansen and McDonald, 1986) [7] one introduces the space-time Fourier transform, $\chi(\mathbf{k},\omega)$, of the linear density response function. Which is related through the fluctuation dissipation theorem, $S(\mathbf{k},\omega) = -(2\hbar/n)\Theta(\omega)\mathrm{Im}\chi(\mathbf{k},\omega)$, to the space-time Fourier transform, $S(\mathbf{k},\omega)$ (dynamic structure factor), of the van Hove correlation function (van Hove, 1954), $\langle\rho(\mathbf{r},t)\rho(\mathbf{0},0)\rangle/n$, where $\rho(\mathbf{r},t) = \exp(iHt/\hbar)\rho(\mathbf{r})\exp(-iHt/\hbar)$.

In the Random Phase Approximation (RPA) we have (Pines and Nozières, 1966)

$$\frac{1}{\chi_{RPA}(k,\omega)} = \frac{1}{\chi_0(k,\omega)} - e^2\tilde{v}_\mu(k) \ , \tag{C1}$$

where χ_0 is the response function of the non-interacting Fermions (ideal Fermi gas), known as the Lindhard susceptibility (Lindhard, 1954). This corresponds to taking the "proper polarizability" (the response to the Hartree potential) equal to the response of the ideal Fermi gas (Tosi, 1999). With the help of the fluctuation dissipation theorem, $S_0(k,\omega) = -(2\hbar/n)\Theta(\omega)\mathrm{Im}\chi_0(k,\omega)$ gives the differential cross-section for inelastic scattering from the ideal Fermi gas (at energy transfer $\omega \geq 0$). Scattering is due to the excitation of single particle-hole pairs

$$S_0(k,\omega) = 2\pi\sum_{\mathbf{q},\sigma} n^0_{\mathbf{q}}[1-n^0_{\mathbf{q}+\mathbf{k}}]\delta\left[\omega - \frac{1}{\hbar}(e_{\mathbf{q}+\mathbf{k}} - e_{\mathbf{q}})\right] \ , \tag{C2}$$

where $e_{\mathbf{k}} = \hbar^2k^2/(2m)$ and $n^0_{\mathbf{k}} = \Theta(|\mathbf{k}| - k_F)$ is the momentum distribution of the ideal Fermi gas. We thus find

$$S_0(k,\omega) = \begin{cases} \hbar\pi\nu_F\frac{\omega}{kv_F} & 0 \leq \omega \leq -\omega_2(k) \\ \hbar\pi\nu_F\frac{k_F}{2k}\left[1-\left(\frac{\omega}{kv_F}-\frac{k}{2k_F}\right)^2\right] & |\omega_2(k)| \leq \omega \leq \omega_1(k) \\ 0 & \omega \geq \omega_1(k) \end{cases} \tag{C3}$$

with $\nu_F = mk_F/(n\pi^2\hbar^2)$ the density of states for particles at the Fermi level, $v_F = \hbar k_F/m$ the velocity of a free particle on the Fermi surface, $\omega_1(k) = \hbar(kk_F + k^2/2)/m$, and $\omega_2(k) = \hbar(-kk_F + k^2/2)/m$. Naturally we also have $S^x(k) = \int S_0(k,\omega)d\omega/(2\pi)$.

The RPA static structure factor is then recovered through

$$S_{RPA}(k) = -\frac{\hbar}{n}\int_0^\infty \frac{d\omega}{\pi}\,\mathrm{Im}\chi(k,\omega) \ . \tag{C4}$$

where

$$\mathrm{Im}\chi = \frac{\mathrm{Im}\chi_0}{(1-e^2\tilde{v}_\mu\mathrm{Re}\chi_0)^2 + (e^2\tilde{v}_\mu\mathrm{Im}\chi_0)^2} \ , \tag{C5}$$

and

$$\mathrm{Im}\chi_0 = -\frac{n}{2\hbar}S_0 \ , \quad \omega > 0 \ , \tag{C6}$$

$$\mathrm{Re}\chi_0 = -n\nu_F\left\{\frac{1}{2} + \frac{1-(x-y)^2}{8y}\ln\left|\frac{x-1-y}{x+1-y}\right| + \frac{1-(x+y)^2}{8y}\ln\left|\frac{x+1+y}{x-1+y}\right|\right\} \ , \tag{C7}$$

where $x = \omega/kv_F$ and $y = k/2k_F$. In deriving Eq. (C7) we used the fact that $\mathrm{Im}\chi_0(k,\omega)$ is an odd function of ω and the Kramers-Kronig relations.

Appendix D: Analytic expressions for the non-interacting fermions ground state

Usually $g_{\sigma,\sigma'}$ is conventionally divided into the (known) exchange and the (unknown) correlation terms

$$g_{\sigma,\sigma'} = g^x_{\sigma,\sigma'} + g^c_{\sigma,\sigma'} \ , \tag{D1}$$

where the exchange term corresponds to the uniform system of non-interacting fermions.

---

[7] Note that, unlike in the classical case, in quantum statistical physics even the linear response to a *static* perturbation requires the use of imaginary time correlation functions (Martin, 1988).

1. Radial distribution function

We thus have (from the definition of the RDF (2.37) and using Slater determinants for the wave-function)

$$g^x_{+,-}(r) = 1 \ , \tag{D2}$$

$$g^x_{\sigma,\sigma}(r) = 1 - \left[\frac{3j_1(k_F^\sigma r)}{k_F^\sigma r}\right]^2 \ , \tag{D3}$$

where $j_1(x) = [\sin(x) - x\cos(x)]/x^2$ is the spherical Bessel function of the first kind and $(k_F^\sigma)^3 = 6\pi^2 n_\sigma$ is the Fermi wave-number for particles of spin σ.

2. Static structure factor

Again we will have the splitting $S_{\sigma,\sigma'} = S^x_{\sigma,\sigma'} + S^c_{\sigma,\sigma'}$ into the exchange and the correlation parts. So that for the non-interacting fermions we get

$$S^x_{+,-}(k) = 0 \ , \tag{D4}$$

$$\begin{aligned} S^x_{\sigma,\sigma}(k) &= \frac{n_\sigma}{n} - \frac{n_\sigma^2}{n}\Theta(2k_F^\sigma - k)\frac{3\pi^2}{(k_F^\sigma)^3}\left(1 - \frac{k}{2k_F^\sigma}\right)^2\left(2 + \frac{k}{2k_F^\sigma}\right) \\ &= \frac{n_\sigma}{n}\begin{cases} 1 & k > 2k_F^\sigma \\ \frac{3}{4}\frac{k}{k_F^\sigma} - \frac{1}{16}\left(\frac{k}{k_F^\sigma}\right)^3 & k < 2k_F^\sigma \end{cases} , \end{aligned} \tag{D5}$$

where $\Theta(x)$ is the Heaviside step function.

3. Internal energy

The Hartree-Fock approximation (Fock, 1930; Hartree, 1928; Slater, 1930) for the ground state of a system of interacting fermions assumes that the many-body wave function is a Slater determinant built from single-particle states, which are to be determined self-consistently by minimization of the expectation value of the Hamiltonian. Whereas for an inhomogeneous many-electron system (e.g. an atom or a molecule) the solution of the Hartree-Fock self-consistent problem can usually be obtained only in a numerical form involving further approximations, the exact Hartree-Fock solution is immediate in the case of a homogeneous fluid: in this case the self-consistent single-particle states are necessarily plane waves, from translational invariance. Hence, the Hartree-Fock wave function for the ground-state of a homogeneous fluid is the same as the ground-state wave function of the ideal Fermi gas.

Including explicitly the spin indices we get

$$E_g^{\rm HF} = \sum_{\mathbf{k},\sigma} n^0_{\mathbf{k},\sigma}\left[\epsilon_{\mathbf{k}} + \frac{1}{2}\Sigma_{HF}(\mathbf{k})\right], \tag{D6}$$

where $n^0_{\mathbf{k},\sigma}$ is the ideal Fermi distribution, $\epsilon_{\mathbf{k}} = \hbar^2k^2/2m$ and for an unpolarized system

$$\Sigma_{\rm HF}(\mathbf{k}) = v_0 + \frac{1}{N}\sum_{\mathbf{q}} v_{\mathbf{q}} n^0_{\mathbf{k}+\mathbf{q},\sigma} \tag{D7}$$

$$= -\frac{e^2k_F}{\pi}\left[1 + \frac{k_F^2 - k^2}{2kk_F}\ln\left|\frac{k+k_F}{k-k_F}\right|\right], \tag{D8}$$

here $v_0 = v_{\mathbf{q}=\mathbf{0}}$ and $v_{\mathbf{q}} = 4\pi e^2/q^2$. So that

$$e_g^{\rm HF} = E_g^{\rm HF}/N = \left(\frac{3}{5\alpha^2 r_s^2} - \frac{3}{2\pi\alpha r_s}\right){\rm Ry} = \left(\frac{2.21}{r_s^2} - \frac{0.916}{r_s}\right){\rm Ry}, \tag{D9}$$

with $\alpha = (9\pi/4)^{-1/3}$. As already remarked, the gain in potential energy found in Hartree-Fock derives from the fact that the exclusion principle is built into the many-body wave function and keeps apart pairs of electrons with parallel spins, thus lowering their Coulomb repulsive interaction energy on average. Notice that the ratio between potential and kinetic energy is proportional to r_s: this dimensionless length gives a measure of the coupling strength,

which increases with decreasing density. The main problem with the Hartee-Fock approximation is that, by including exchange between electrons with parallel spins but neglecting correlations due to the Coulomb repulsions (which are most effective for electrons with antiparallel spins), it includes neither dielectric screening nor the collective plasma excitation. As shown in section II.D.2 the Hartree-Fock ground-state can be determined from the exchange part of the radial distribution function (see Eqs. (D2)-(D3)).

When one proceeds to evaluate the ground-state energy of Jellium by perturbation theory beyond first order (i.e. beyond Hartree-Fock), one meets divergences arising from the long-range character of the Coulomb interactions. On summing to infinite order the most strongly divergent terms of the perturbative expansion (corresponding to the RPA theory), screening introduces a cut-off as the lower end of integrals over wave vector space and cures the divergences (Gell-Mann and Bruckner, 1957). Such a calculation, supplemented by the inclusion of a contribution from second-order exchange processes, yields the low r_s expansion

$$e_g(r_s) = \left[\frac{2.21}{r_s^2} - \frac{0.916}{r_s} + 0.0622 \ln r_s - 0.096 + \dots\right] \text{Ry}, \tag{D10}$$

plus terms going like r_s, $r_s \ln r_s$, etc. The results of such a truncated expansion is reasonably accurate only up to $r_s = 1$, whereas the values of r_s that are relevant in the physics of normal metals extend up to $r_s = 6$.

In the thirties Wigner (Wigner, 1938a,b) had already noticed that an optimal value $e_{\rm pot} = -(1.8/r_s)$Ry is obtained for the potential energy if the electrons are placed on the sites of a crystalline lattice having body-centered-cubic (bcc) structure. The gain by a factor ≈ 2 over the potential energy in Hartree-Fock is clearly related to the fact that in the crystal all pairs of electrons keep apart irrispectively of their relative spin orientation. Using the crystalline result at large r_s in combination with an estimate of the correlation energy at low r_s, Wigner proposed the interpolation formula

$$e_g^{\rm W} = \left[\frac{2.21}{r_s^2} - \frac{0.916}{r_s} - \frac{0.88}{7.8 + r_s}\right] \text{Ry}, \tag{D11}$$

as approximately valid at metallic densities.

Appendix E: Radial distribution functions sum rules in the ground state

Both the behavior of the RDF at small r and at large r has to satisfy to general exact relations or sum rules.

1. Cusp conditions

When two electrons ($\mu = \infty$) get closer and closer together, the behavior of $g_{\sigma,\sigma'}(r)$ is governed by the exact cusp conditions (Hoffmann-Ostenhof *et al.*, 1992; Kimball, 1973; Rajagopal *et al.*, 1978)

$$\left.\frac{d}{dr} g_{\sigma,\sigma}(r)\right|_{r\to 0} = 0 \ , \tag{E1}$$

$$\left.\frac{d^3}{dr^3} g_{\sigma,\sigma}(r)\right|_{r\to 0} = \frac{3}{2a_0} \left.\frac{d^2}{dr^2} g_{\sigma,\sigma}(r)\right|_{r\to 0} \ , \tag{E2}$$

$$\left.\frac{d}{dr} g_{+,-}(r)\right|_{r\to 0} = \frac{1}{a_0} g_{+,-}(0) \ , \tag{E3}$$

where in the adimensional units $a_0 \to 1/r_s$. For finite μ we only have the condition $g_{\sigma,\sigma}(0) = 0$ due to Pauli exclusion principle.

2. The Random Phase Approximation (RPA) and the long range behavior of the RDF

The small k behavior of the RPA, summarized in Appendix C, is exact (Pines and Nozières, 1966). One finds

$$S_{RPA}(k) = \frac{\hbar k^2}{2m\omega_p} \ , \quad k \ll k_F \ , \tag{E4}$$

where $\omega_p = \sqrt{4\pi n e^2/m}$ is the plasmon frequency (Giuliani and Vignale, 2005). This is also known as the second-moment sum rule for the exact RDF and can be rewritten as $n \int d\mathbf{r}\, r^2 [g(r) - 1] = -6(\hbar/2m\omega_p)$. We can then say

that $g(r) - 1$ has to decay faster than r^{-5} at large r. The fourth-moment (or compressibility) sum rule links the thermodynamic compressibility, $\chi = [nd(n^2 de_0/dn)/dn]^{-1}$, (Tosi, 1999) to the fourth-moment of the RDF. For the equivalent classical system it is well known that the correlation functions have to decay faster than any inverse power of the distance (Alastuey and Martin, 1985; Lighthill, 1959; Martin, 1988) (in accord with the Debye-Hükel theory). To the best of our knowledge we do not know, yet, the exact decay for the zero temperature quantum case.

Appendix F: The primitive action

Suppose the Hamiltonian is split into two pieces $\mathcal{H} = \mathcal{T}+\mathcal{V}$, where *calt* and $\mathcal{V}$ are the kinetic and potential operators. Recall the exact Baker-Campbell-Hausdorff formula to expand $\exp(-\tau\mathcal{H})$ into the product $\exp(-\tau\mathcal{T})\exp(-\tau\mathcal{V})$. As $\tau \to 0$ the commutator terms which are of order higher than τ^2 become smaller than the other terms and thus can be neglected. This is known as the *primitive approximation*

$$e^{-\tau(\mathcal{T}+\mathcal{V})} \approx e^{-\tau\mathcal{T}} e^{-\tau\mathcal{V}}. \tag{F1}$$

hence we can approximate the exact density matrix by product of the density matrices for $\mathcal{T}$ and $\mathcal{V}$ alone. One might worry that this would lead to an error as $M \to \infty$, with small errors building up to a finite error. According to the Trotter (Trotter, 1959) formula, one does not have to worry

$$e^{-\beta(\mathcal{T}+\mathcal{V})} = \lim_{M\to\infty} \left[e^{-\tau\mathcal{T}} e^{-\tau\mathcal{V}}\right]^M. \tag{F2}$$

The Trotter formula holds if the three operators $\mathcal{T}$, $\mathcal{V}$, and $\mathcal{T}+\mathcal{V}$ are self-adjoint and make sense separately, for example, if their spectrum is bounded below (Simon, 1979). This is the case for the Hamiltonian describing Jellium.

Let us now write the primitive approximation in position space

$$\rho(R_0, R_2; \tau) \approx \int dR_1 \langle R_0|e^{-\tau\mathcal{T}}|R_1\rangle\langle R_1|e^{-\tau\mathcal{V}}|R_2\rangle, \tag{F3}$$

and evaluate the kinetic and potential density matrices. Since the potential operator is diagonal in the position representation, its matrix elements are trivial

$$\langle R_1|e^{-\tau\mathcal{V}}|R_2\rangle = e^{-\tau V(R_1)}\delta(R_2 - R_1). \tag{F4}$$

The kinetic matrix can be evaluated using the eigenfunction expansion of $\mathcal{T}$. Consider, for example, the case of distinguishable particles in a cube of side L with periodic boundary conditions. Then the exact eigenfunctions and eigenvalues of $\mathcal{T}$ are $L^{-3N/2}e^{iK_{\mathbf{n}}R}$ and $\lambda K_{\mathbf{n}}^2$, with $K_{\mathbf{n}} = 2\pi\mathbf{n}/L$ and $\mathbf{n}$ a $3N$-dimensional integer vector. We are using here dimensional units. Then

$$\langle R_0|e^{-\tau\mathcal{T}}|R_1\rangle = \sum_{\mathbf{n}} L^{-3N} e^{-\tau\lambda K_{\mathbf{n}}^2} e^{-iK_{\mathbf{n}}(R_0-R_1)} \tag{F5}$$

$$= (4\pi\lambda\tau)^{-3N/2} \exp\left[-\frac{(R_0-R_1)^2}{4\lambda\tau}\right], \tag{F6}$$

where $\lambda = \hbar^2/2m$. Eq. (F6) is obtained by approximating the sum by an integral. This is appropriate only if the thermal wavelength of one step is much less than the size of the box, $\lambda\tau \ll L^2$. In some special situations this condition could be violated, in which case one should use Eq. (F5) or add periodic "images" to Eq. (F6). The exact kinetic density matrix in periodic boundary conditions is a theta function, $\prod_{i=1}^{3N}\theta_3(z_i, q)$, where $z = \pi(R_0^i - R_1^i)/L$, R^i is the ith component of the $3N$ dimensional vector R, and $q = e^{-\lambda\tau(2\pi/L)^2}$ (see chapter 16 of Ref. (Abramowitz and Stegun, 1970)). Errors from ignoring the boundary conditions are $O(q)$, exponentially small at large M.

A *link* m is a pair of time slices (R_{m-1}, R_m) separated by a *time step* $\tau = \beta/M$. The *action* S^m of a link is defined as minus the logarithm of the exact density matrix. Then the exact path-integral expression becomes

$$\rho(R_0, R_M; \beta) = \int dR_1 \ldots dR_{M-1} \exp\left[-\sum_{m=1}^{M} S^m\right], \tag{F7}$$

It is convenient to separate out the *kinetic action* from the rest of the action. The exact kinetic action for link m will be denoted K^m

$$K^m = \frac{3N}{2}\ln(4\pi\lambda\tau) + \frac{(R_{m-1}-R_m)^2}{4\lambda\tau}, \tag{F8}$$

The *inter-action* is then defined as what is left

$$U^m = U(R_{m-1}, R_m; \tau) = S^m - K^m. \tag{F9}$$

In the primitive approximation the inter-action is

$$U_1^m = \frac{\tau}{2}[V(R_{m-1}) + V(R_m)], \tag{F10}$$

where we have symmetrized U_1^m with respect to R_{m-1} and R_m, since one knows that the exact density matrix is symmetric and thus the symmetrized form is more accurate.

A capital letter U refers to the total link inter-action. One should not think of the exact U as being strictly the potential action. That is true for the primitive action but, in general, is only correct in the small-τ limit. The exact U also contains kinetic contributions of higher order in τ. If a subscript is present on the inter-action, it indicates the order of approximation; the primitive approximation is only correct to order τ. No subscript implies the exact inter-action.

The *residual energy* of an approximate density matrix is defined as

$$E_A(R, R'; t) = \frac{1}{\rho_A(R, R'; t)} \left[\mathcal{H} + \frac{\partial}{\partial t}\right] \rho_A(R, R'; t). \tag{F11}$$

The residual energy for an exact density matrix vanishes; it is a local measure of the error of an approximate density matrix. The Hamiltonian $\mathcal{H}$ is a function of R; thus the residual energy is not symmetric in R and R'.

It is useful to write the residual energy as a function of the inter-action. We find

$$E_A(R, R'; t) = V(R) - \frac{\partial U_A}{\partial t} - \frac{(R - R') \cdot \nabla U_A}{t} + \lambda \nabla^2 U_A - \lambda \left(\nabla U_A\right)^2. \tag{F12}$$

The terms on the right hand side are ordered in powers of τ, keeping in mind that $U(R)$ is of order τ, and $|R - R'|$ is of order $\tau^{1/2}$. One obtains the primitive action by setting the residual energy to zero and dropping the last three terms on the right hand side.

The residual energy of the primitive approximation is

$$E_1(R, R'; t) = \frac{1}{2}\left[V(R) - V(R')\right] - \frac{1}{2}(R - R') \cdot \nabla V + \frac{\lambda t}{2}\nabla^2 V - \frac{\lambda t^2}{4}\left(\nabla V\right)^2. \tag{F13}$$

With a leading error of $\sim \lambda \tau^2$.

Appendix G: The pair-product action

An often useful method to determine the many-body action is to use the exact action for two electrons (Barker, 1979). To justify this approach, first assume that the potential energy can be broken into a pairwise sum of terms

$$V(R) = \sum_{i<j} v(|\mathbf{r}_i - \mathbf{r}_j|), \tag{G1}$$

with $|\mathbf{r}_i - \mathbf{r}_j| = r_{ij}$. Next, apply the Feynman-Kac formula for the inter-action

$$e^{-U(R_0, R_F; \tau)} = \left\langle \exp\left[-\int_0^\tau dt\, V(R(t))\right]\right\rangle_{\mathrm{RW}}, \tag{G2}$$

where the notation $\langle \ldots \rangle_{\rm RW}$ means the average over all Gaussian random walks from R_0 to R_F in a "time" τ. So that

$$e^{-U(R_0,R_F;\tau)} = \left\langle \exp\left[-\int_0^\tau dt \sum_{i<j} v(r_{ij}(t))\right]\right\rangle_{\rm RW} \tag{G3}$$

$$= \left\langle \prod_{i<j} \exp\left[-\int_0^\tau dt\, v(r_{ij}(t))\right]\right\rangle_{\rm RW} \tag{G4}$$

$$\approx \prod_{i<j} \left\langle \exp\left[-\int_0^\tau dt\, v(r_{ij}(t))\right]\right\rangle_{\rm RW} \tag{G5}$$

$$= \prod_{i<j} \exp\left[-u_2(r_{ij}, r'_{ij};\tau)\right] \tag{G6}$$

$$= \exp\left[-\sum_{i<j} u_2(r_{ij}, r'_{ij};\tau)\right] = e^{-U_2(R_0,R_F;\tau)}, \tag{G7}$$

where U_2 is the *pair-product* action and u_2 is the exact action for a pair of electrons. At low temperatures the pair action approaches the solution of the two particle wave equation. The result is the pair-product or Jastrow ground-state wave function, which is the ubiquitous choice for a correlated wave function because it does such a good job of describing most ground-state correlations.

The residual energy (see Eq. (F11)) for the pair-product action is less singular than for other forms. We have that

$$u_2(r_{ij}, r'_{ij};\tau) = -\ln\left\langle \exp\left(-\int_0^\tau dt\, v(r_{ij}(t))\right)\right\rangle_{\rm RW}, \tag{G8}$$

is of order τ^2 since the two body problem can be factorized into a center-of-mass term and a term that is a function of the relative coordinates. Moreover we must have

$$\frac{\partial u_2}{\partial \tau} = v(r_{ij}(\tau)), \tag{G9}$$

so that

$$\frac{\partial U_2}{\partial \tau} = V(R(\tau)), \tag{G10}$$

which tells that only the last three terms on the right hand side of Eq. (F12) contribute to the residual energy. We also have

$$\nabla U_2 = \sum_i \sum_{i\neq j} \nabla_i u_2(r_{ij}, r'_{ij};\tau), \tag{G11}$$

where the indices run over the particles. So the leading error of the pair-product action is $\sim \lambda\tau^3$.

ACKNOWLEDGMENTS

REFERENCES

Abramowitz, M., and I. A. Stegun (1970), *Handbook of mathematical functions* (Dover, New York).
Alastuey, A., and P. A. Martin (1985), J. Stat. Phys. **39**, 405.
Allen, M. P., and D. J. Tildesley (1987), *Computer Simulation of Liquids* (Clarendon Press, Oxford).
Anderson, J. B. (1976), J. Chem. Phys. **65**, 4121.
Ashcroft, N. W., and N. D. Mermin (1976), *Solid State Physics* (Harcourt, Inc., Forth Worth).
Assaraf, R., and M. Caffarel (2003), J. Chem. Phys. **119**, 10536.
Barker, J. A. (1979), J. Chem. Phys. **70**, 2914.
Barnett, R. N., P. J. Reynolds, and J. W. A. Lester (1991), J. Comp. Phys. **96**, 258.
Baroni, S., and S. Moroni (1999), Phys. Rev. Lett. **82**, 4745.
Bijl, A. (1940), Physica **7**, 869.
Boninsegni, M., N. Prokof'ev, and B. Svistunov (2006), Phys. Rev. Lett. **96**, 070601.
Brown, E., M. A. Morales, C. Pierleoni, and D. M. Ceperley (2014), in *Frontiers and Challenges in Warm Dense Matter*, edited by F. G. *et al.* (Springer) pp. 123–149.

Brown, E. W., B. K. Clark, J. L. DuBois, and D. M. Ceperley (2013), Phys. Rev. Lett. **110**, 146405.
Ceperley, D. M. (1978), Phys. Rev. B **18**, 3126.
Ceperley, D. M. (1991), J. Stat. Phys. **63**, 1237.
Ceperley, D. M. (1995), Rev. Mod. Phys. **67**, 279.
Ceperley, D. M. (1996), in *Monte Carlo and Molecular Dynamics of Condensed Matter Systems*, edited by K. Binder and G. Ciccotti (Editrice Compositori, Bologna, Italy).
Ceperley, D. M. (2004), in *Proceedings of the International School of Physics Enrico Fermi*, edited by G. F. Giuliani and G. Vignale (IOS Press, Amsterdam) pp. 3–42, course CLVII.
Ceperley, D. M., and B. J. Alder (1980), Phys. Rev. Lett. **45**, 566.
Ceperley, D. M., M. Dewing, and C. Pierleoni (2002), in *Bridging Time Scales: Molecular Simulations for the Next Decade* (Springer-Verlag) pp. 473–500.
Ceperley, D. M., and M. H. Kalos (1979), in *Monte Carlo Methods in Statistical Physics*, edited by K. Binder (Springer-Verlag, Heidelberg) p. 145.
Chiesa, S., D. M. Ceperley, R. M. Martin, and M. Holzmann (2006), Phys. Rev. Lett. **97**, 076404.
Dewing, M., and D. M. Ceperley (2002), in *Recent Advances in Quantum Monte Carlo Methods*, edited by W. A. Lester, S. M. Rothstein, and S. Tanaka (World Scientific, Singapore).
Dharma-wardana, M. W. C., and F. Perrot (2000), Phys. Rev. Lett. **84**, 959.
Dingle, R. B. (1949), Philos. Mag. **40**, 573.
Dornheim, T., S. Groth, T. Sjostrom, F. D. Malone, W. M. C. Foulkes, and M. Bonitz (2016), Phys. Rev. Lett. **117**, 156403.
Dutta, S., and J. Dufty (2013), Phys. Rev. E **87**, 032102.
Ernstorfer, R. *et al.*. (2009), Science **323**, 5917.
Fantoni, R. (2013), Solid State Communications **159**, 106.
Feenberg, E. (1967), *Theory of Quantum Fluids* (Academic Press).
Feynman, R. P. (1953a), Phys. Rev. **90**, 1116.
Feynman, R. P. (1953b), Phys. Rev. **91**, 1291.
Feynman, R. P. (1953c), Phys. Rev. **90**, 1301.
Feynman, R. P. (1972), *Statistical Mechanics: A Set of Lectures* (W. A. Benjamin Inc., London, Amsterdam, Don Mills, Sydney, Tokyo) section 9.6.
Feynman, R. P., and M. Cohen (1956), Phys. Rev. **102**, 1189.
Feynman, R. P., and A. R. Hibbs (1965), *Quantum Mechanics and Path Integrals* (McGraw-Hill Publishing Company, New York) page 292-293.
Fletcher, L. B. *et al.*. (2014), Phys. Rev. Lett. **112**, 145004.
Fock, V. (1930), Zs. Phys. **61**, 126.
Foulkes, W. M. C., L. Mitas, R. J. Needs, and G. Rajagopal (2001), Rev. Mod. Phys. **73**, 33.
Gaskell, T. (1961), Proc. Phys. Soc. **77**, 1182.
Gaskell, T. (1962), Proc. Phys. Soc. **80**, 1091.
Gaudoin, R., and J. M. Pitarke (2007), Phys. Rev. Lett. **99**, 126406.
Gell-Mann, M., and K. A. Bruckner (1957), Phys. Rev. **106**, 364.
Giuliani, G. F., and G. Vignale (2005), *Quantum Theory of the Electron Liquid* (Cambridge University Press, Cambridge).
Grimes, C. C., and G. Adams (1979), Phys. Rev. Lett. **42**, 795.
Gupta, U., and A. K. Rajagopal (1980), Phys. Rev. A **22**, 2792.
Hammersley, J. M., and D. C. Handscomb (1964), *Monte Calro Methods* (Chapman and Hall, London) pp. 57-59.
Hansen, J. P. (1973), Phys. Rev. A **8**, 3096.
Hansen, J. P., and I. R. McDonald (1986), *Theory of simple liquids*, 2nd ed. (Academic Press, London).
Hansen, J. P., and P. Vieillefosse (1975), Phys. Lett. **53A**, 187.
Hartree, D. R. (1928), Proc. Cambridge Phil. Soc. **24**, 89 and 111.
Hill, T. L. (1956), *Statistical Mechanics* (McGraw-Hill, New York).
Hoffmann-Ostenhof, M., T. Hofmann-Ostenhof, and H. Stremnitzer (1992), Phys. Rev. Lett. **68**, 3857.
van Hove, L. (1954), Phys. Rev. **95**, 249.
Ichimaru, S. (1982), Rev. Mod. Phys. **54**, 1017.
Jancovici, B. (1978), Physica (Amsterdam) **91A**, 152.
Jastrow, R. (1955), Phys. Rev. **98**, 1479.
Jones, M. D., and D. M. Ceperley (1996), Phys. Rev. Lett. **76**, 4572.
Kac, M. (1951) (University of California Press, Berkeley) sec. 3.
Kac, M. (1959), *Probability and Related Topics in Physical Sciences* (Interscience Publisher Inc., New York).
Kalos, M. H., D. Levesque, and L. Verlet (1974), Phys. Rev. A **9**, 2178.
Kalos, M. H., and P. A. Whitlock (2008), *Monte Carlo Methods* (Wiley-Vch Verlag GmbH & Co., Germany).
Kimball, J. C. (1973), Phys. Rev. A **7**, 1648.
Knudson, M. D. *et al.*. (2012), Phys. Rev. Lett. **108**, 091102.
Kolorenc, J., and L. Mitas (2011), Rep. Prog. Phys. **74**, 026502.
Kwon, Y., D. M. Ceperley, and R. M. Martin (1993), Phys. Rev. B **48**, 12037.
Kwon, Y., D. M. Ceperley, and R. M. Martin (1998), Phys. Rev. B **58**, 6800.
Landau, L. D., and E. M. Lifshitz (1951), *Statistical Physics*, Course of Theoretical Physics, Vol. 5 (Butterworth Heinemann) translated from the Russian by J. B. Sykes and M. J. Kearsley, edited by E. M. Lifshitz and L. P. Pitaevskii.

Landau, L. D., and E. M. Lifshitz (1977), *Quantum Mechanics. Non-relativistic Theory*, 3rd ed., Vol. 3 (Pergamon Press) course of Theoretical Physics. Eq. (11.16).
Leggett, A. J. (1975), Rev. Mod. Phys. **47**, 331.
Lighthill, M. J. (1959), *Introduction to Fourier Analysis and Generalized Functions* (Cambridge University Press) theorem 19.
Lin, C., F. H. Zong, and D. M. Ceperley (2001), Phys. Rev. E **64**, 016702.
Lindhard, J. (1954), Mat.-Fys. Medd. **28** (8).
Liu, K. S., M. H. Kalos, and G. V. Chester (1974), Phys. Rev. A **10**, 303.
March, N. H. (1990), *Liquid Metals – Concepts and theory* (Cambridge University Press, Cambridge).
March, N. H., and M. P. Tosi (1984), *Coulomb Liquids* (Academic Press, London).
March, N. H., and M. P. Tosi (2002), *Introduction to liquid state physics* (World Scientific, Singapore).
Martin, P. A. (1988), Rev. Mod. Phys. **60**, 1075.
Mazzola, G., S. Yunoki, and S. Sorella (2014), Nat. Commun. **5**, 3487.
Metropolis, N., A. W. Rosenbluth, M. N. Rosenbluth, A. M. Teller, and E. Teller (1953), J. Chem. Phys. **1087**, 21.
Natoli, V., and D. M. Ceperley (1995), Comput. Phys. **117**, 171.
Ortiz, G., and P. Ballone (1994), Phys. Rev. B **50**, 1391.
Panoff, R. M., and J. Carlson (1989), Phys. Rev. Lett. **62**, 1130.
Paziani, S., S. Moroni, P. Gori-Giorgi, and G. B. Bachelet (2006), Phys. Rev. B **73**, 155111.
Perdew, J. P., and A. Zunger (1981), Phys. Rev. B **23**, 5048.
Perrot, F., and M. W. C. Dharma-wardana (1984), Phys. Rev. A **30**, 2619.
Perrot, F. M. C., and M. W. C. Dharma-wardana (2000), Phys. Rev. B **62**, 16536.
Pines, D., and P. Nozières (1966), *Theory of Quantum Liquids* (Benjamin, New York).
Pollock, E. L. (1988), Computer Physics Communications **52**, 49.
Pollock, E. L., and D. M. Ceperley (1987), Phys. Rev. B **36**, 8343.
Pollock, E. L., and J. P. Hansen (1973), Phys. Rev. A **8**, 3110.
Rajagopal, A. K., J. C. Kimball, and M. Banerjee (1978), Phys. Rev. B **18**, 2339.
Shapiro, S. L., and S. A. Teukolsky (1983), *Black Holes, White Dwarfs, and Neutron Stars. The Physics of Compact Objects* (John Wiley & Sons, Inc., Germany).
Simon, B. (1979), *Functional integration and quantum physics* (Academic, New York).
Singwi, K. S., and M. P. Tosi (1981), Sol. State Phys. **36**, 177.
Singwi, K. S., M. P. Tosi, R. H. Land, and A. Sjölander (1968), Phys. Rev. **176**, 589.
Slater, J. C. (1930), Phys. Rev. **35**, 210.
Tanaka, S., and S. Ichimaru (1986), Journal of the Physical Society of Japan **55**, 2278.
Tanatar, B., and D. M. Ceperley (1989), Phys. Rev. B **39**, 5005.
Tosi, M. P. (1999), in *Electron Correlation in the Solid State*, edited by N. H. March, Chap. 1 (Imperial College Press, London) pp. 1–42.
Toulouse, J., R. Assaraf, and C. J. Umrigar (2007), J. Chem. Phys. **126**, 244112.
Trotter, H. F. (1959), Proc. Am. Math. Soc. **10**, 545.
Umrigar, C. J., M. P. Nightingale, and K. J. Runge (1993), J. Chem. Phys. **99**, 2865.
Vieillefosse, P. (1994), J. Stat. Phys. **74**, 1195.
Vieillefosse, P. (1995), J. Stat. Phys. **80**, 461.
Wigner, E. (1934), Phys. Rev. **46**, 1002.
Wigner, E. P. (1938a), Phys. Rev. **46**, 1002.
Wigner, E. P. (1938b), Trans. Faraday Soc. **34**, 678.